PHILOSOPHICAL TRANSACTIONS OF THE ROYAL SOCIETY A MATHEMATICAL, PHYSICAL & ENGINEERING SCIENCES

Rapid Force-Flux Transitions in Highly Porous Membranes

P. Meares and K. R. Page

Phil. Trans. R. Soc. Lond. A 1972 **272**, 1-46
doi: 10.1098/rsta.1972.0031

RAPID FORCE-FLUX TRANSITIONS IN HIGHLY POROUS MEMBRANES

By P. MEARES and K. R. PAGE
Department of Chemistry, University of Aberdeen

(*Communicated by R. M. Barrer, F.R.S.* – *Received* 26 *April* 1971 – *Revised* 23 *August* 1971)

CONTENTS

Vol. 272 A. 1219. (Price £1.20; U.S. $3.35) 1 [Published 24 February 1972

When a steady electric current is passed through a porous membrane which separates two electrolyte solutions at different concentrations the system can, in a suitable experimental configuration, enter a state of stable oscillations of the trans-membrane pressure and potential. This system, sometimes called the Teorell membrane oscillator, also displays unusual stationary state behaviour when the pressure difference across the membrane is held constant. These phenomena arise because the pressure-driven flow of volume through the membrane is virtually independent of the concentration of the solution in its pores, whereas the electro-osmotic flow decreases as the concentration increases. If the pressure-driven and electro-osmotic flows are opposed and pressure is applied to the concentrated solution then at low currents pressure drives the concentrated solution into the pores and at high currents electro-osmosis drags the dilute solution into the pores. At some intermediate current the transition from concentrated to dilute solution in the pores occurs and is accompanied by a sudden increase in the membrane resistance and potential difference.

These observations have been made on various membranes of ill-defined structure, it is shown here that they can be reproduced with Nuclepore filters which have readily characterized uniform circular and parallel pores. This observation has facilitated the development and testing of a quantitative theory of the phenomenon.

The theory developed here follows the lines laid down by Kobatake & Fujita (1964) and by Mikulecky & Caplan (1966). The membrane pores are treated as independent capillaries lined by an electrical double layer with a diffuse counter charge in the pore solution. A system of flux equations consistent with non-equilibrium thermodynamics is developed and the minimum assumptions and idealizations needed to obtain well-defined results are identified. Flow in the pores is treated via the Navier–Stokes equation and equations for the membrane fluxes and forces are obtained in terms of the membrane properties and external parameters under the control of an experimenter.

Two cases are considered. In the first the surface charge density on the pore walls is independent of the solution concentration and in the second the surface charge density is proportional to the cube root of the concentration. The second case applies to Nuclepore membranes because the surface charge on polycarbonate is probably due mainly to adsorption of anions from solution. In the first case the electro-osmotic flow is inversely proportional to the one-half power of the concentration and in the second case to the one-sixth power.

In order to convert the barycentric local flux equations to equations describing the macroscopic phenomena account must be taken of the radial variation of parameters over a pore cross-section and to their variation along the pore from one membrane boundary to the other.

Radial variation is dealt with first by transferring from the barycentric to the membrane-fixed frame. The flux equations are then averaged over the pore cross-section and finally integrated across the membrane under the assumption of a steady state. This procedure has the advantage of producing manageable flux equations, with no adjustable parameters, which can therefore be given an unequivocal test. It has the disadvantage that no information is obtained concerning the precise mechanisms of the sudden transitions between the high and low resistance states. The flux equations predict the observed types of transitions in fluxes and forces and give a correct general picture of the expected behaviour of the system.

In order to devise a quantitative test it is necessary to bear in mind that it is not technically possible to stir bulk solutions very vigorously against the surfaces of a thin porous membrane without exaggerating pore end effects or even pulsing solutions right through the pores. This difficulty has been dealt with by superimposing upon the membrane flux equations, transport equations across Nernst hypothetical diffusion layers at the membrane/solution boundaries.

Methods of computation have been developed which permit the observable behaviour of the system to be predicted in terms of the ascertainable concentration of the bulk solutions. It is interesting to note that, whereas the low power of the concentration dependence of electro-osmosis in Nuclepore membranes, as compared with constant charge membranes, lowers the scale of the expected force–flux transitions, the presence of stagnant solution layers at the membrane faces increases the scale of these transitions.

The quantitative test of this theory has been based on the comparison of observed and predicted current–voltage curves. A membrane cell has been devised in which the solutions are stirred by paddles and pump circulation to give stable and characterizable stirring conditions. An electric current can be passed through the cell but the products from the electrodes are excluded by ion-exchange membranes. The membrane potential can be measured, and controlled with a potentiostat, via probe holes close to the membrane faces. The pressure difference across the membrane can be maintained at a desired level or allowed to fluctuate in attached vertical tubes.

The pore characteristics of the membranes have been measured optically and by studying hydrodynamic and electro-osmotic flows through them.

Teorell-type oscillations and steady-state dynatron-type current–voltage curves have been recorded in membranes of 0.5, 0.8, 1.0 and 2.0 μm p ore diameter at various currents and pressure differentials in the presence of solutions of NaCl at several concentrations, $MgCl_2$ and Na_2SO_4.

Transitions were observed in current–voltage curves at high enough pressures. The curves showed

hysteresis-like loops. They were characterized by the values of the upper or 'flip' current and lower or 'flop' current on the boundaries of the hysteresis loop and by the difference in the cell resistance between the low current and high current states.

Theoretical values were calculated for the flip and flop currents and the resistance changes under the conditions studied experimentally and a direct comparison made.

Within the limits of the assumptions of ideal solutions and of simple diffuse double-layer theory it was found that agreement was satisfactory on all important matters. In particular, factors that decreased the hydrodynamic permeability or increased the electro-osmotic permeability were correctly found to make the system less sensitive to changes of pressure. This was borne out by the response of the membrane system to changes in the membrane pore size and surface charge, to varying the valence type of the electrolyte and to varying the concentrations of the bulk solutions.

Proceeding from this evidence in favour of the correctness of the theory with regard to current–voltage characteristics, it has been possible to make various predictions regarding the behaviour of the volume and ion fluxes through the membrane in the transition region. It has not yet been possible to measure these fluxes and so to test the predictions which emphasize the importance of the volume flux in controlling the nonlinearity of the system.

Notation

a	pore radius
b_{k}	partial specific volume of k
c_{k}	molar concentration of k
d_{G}	density of gas in manometer
d_{i}	density of solution in compartment i
D	parameter defined by equation (2.2.21)
D'	parameter defined by equation (2.2.23)
D_{k}	diffusion coefficient of k
e_{k}	specific electric charge of k
F	Faraday constant
g	gravitational acceleration
G	parameter defined by equation (2.4.4)
h	linear distance
H	parameter defined by equation (2.4.4)
$\boldsymbol{i}$	electric current density
$(\bar{\boldsymbol{i}})_{\mathrm{c}}$	average electric current density in a pore, $\approx \boldsymbol{i}$
I_{m}	electric current per unit membrane area
I_{s}	streaming current per unit membrane area
$\boldsymbol{j}_{\mathrm{k}}$	molar flux density of k relative to pore wall
J_{k}	flux of k per unit membrane area
J_{m}	salt flux per unit membrane area
$\boldsymbol{J}_{\mathrm{k}}$	local barycentric diffusion flux density of k
$(\boldsymbol{J}_{\mathrm{k}})_{\mathrm{c}}$	local flux density of k relative to pore wall
k_{s}	specific conductance of solution
K	surface charge density parameter in equation (2.3.10)
K_P	parameter defined by equation (3.3.4)
l	membrane thickness
L_{jk}	local barycentric phenomenological coefficient
L_{p}	hydrodynamic permeability of short circuited membrane
L'_{p}	hydrodynamic permeability of open circuited membrane

PHILOSOPHICAL TRANSACTIONS OF THE ROYAL SOCIETY A MATHEMATICAL, PHYSICAL & ENGINEERING SCIENCES

M_k	molecular weight of k
N	number of pores per unit area of membrane
p_i	vapour pressure of solution in compartment i
P	local hydrostatic pressure
Q	a parameter of the solution, equation (2.6.2)
r	radial coordinate in a pore
r_m	electric resistance of membrane per unit pore area
r_t	radius of capillary tubes
R	gas constant
R_f	electric resistance of stagnant film per unit area
R_m	electric resistance of membrane per unit area
$\dot{S}$	local rate of entropy production
t	time
t_k	transport number of k
t_I, t_{II}	parameters defined by equation (2.3.18)
T	temperature
u_k	absolute mobility of k
$\boldsymbol{v}$	local barycentric velocity in a pore
$\bar{v}$	average barycentric velocity in a pore
V_m	volume flux per unit membrane area
x	coordinate normal to membrane surface
z_k	number of elementary positive charges per ion k
α	parameter defined by equation (2.3.8)
β	concentration independent factor in κ
Γ	parameter defined by equation (2.3.17)
δ	thickness of stagnant film of solution
ϵ	dielectric constant
η	shear viscosity of solution
κ	Debye–Hückel reciprocal length
Λ	parameter defined by equation (2.2.22)
Λ'	parameter defined by equation (2.2.24)
μ_k	specific chemical potential of k
$\tilde{\mu}_k$	specific electro-chemical potential of k
ν	total number of ions per molecule of salt
ν_k	number of ions of k per molecule of salt
$\mathring{\boldsymbol{\Pi}}^s$	symmetric pressure tensor
ρ_k	mass fraction (concentration) of k
σ	charge density on pore wall
$\phi(r, x)$	potential relative to $\phi_0(x)$ at pore wall
ψ	local electric potential
$\Delta\psi_d$	liquid junction potential

Subscripts

species k: s = salt, 1 = cation, 2 = anion, 3 = water.
compartments i: I = dilute, II = concentrated.

1. Introduction

Periodic transitions can occur under certain conditions in the fluxes through highly porous membranes of low effective internal charge. This phenomenon was first observed by Teorell (1959*a*). The potential and pressure differences across the membrane oscillated when a constant direct current was passed through a glass sinter membrane which separated two sodium chloride solutions at different concentrations. Similar phenomena have been observed also in membranes prepared from powders of quartz or aluminium oxide, and from fine mesh ion-exchanger beads by Franck and his co-workers (Franck 1963, 1967; Drouin 1969; Jancke 1962).

A qualitative phenomenological explanation of these oscillations is not hard to find. An electric potential difference across the membrane generates, in addition to an electric current of ions, an electro-osmotic flow of solution. In the absence of a pressure difference, this flow takes place towards the electrode whose relative potential has the same sign as the charges fixed to the membrane matrix. At a given membrane current the potential difference, and hence the force driving electro-osmosis, is greater when the membrane pores are filled with a dilute than when they are filled with a concentrated solution. Electro-osmotic flow can be just stopped by opposing it with a hydrostatic pressure, called the electro-osmotic pressure, which is therefore greater for a dilute solution than for a concentrated solution in the pores.

In the apparatus devised by Teorell any volume flow through the membrane generates a hydrostatic pressure opposing the flow and directly proportional to the amount of fluid passed. A steady current passed through a membrane bathed by a single solution builds up the stationary electro-osmotic pressure for that solution. When the membrane separates solutions of different concentration, with the electro-osmotic flow directed from the dilute to the concentrated, instead of reaching a stationary state stable oscillations may be set up.

The electro-osmotic flow initially drags dilute solution into the pores causing strong electro-osmosis which generates a hydrostatic pressure acting to reduce this flow. The reduction in flow permits the concentrated solution to diffuse into the membrane pores and lower the membrane potential until a point is attained where the pressure overcomes the effect of electro-osmosis. The volume flow then reverses and the more concentrated solution flows into the membrane pores diminishing further the electro-osmotic pressure. Owing to the construction of the apparatus the reverse flow causes the hydrostatic pressure to fall until the dilute solution begins to diffuse back into the pores. The electro-osmotic pressure then rises again and overcomes the hydrostatic pressure thus initiating a new cycle. The oscillations therefore arise from alternating changes in the concentration of the solution in the pores.

Characteristic nonlinear stationary state properties are associated with this type of oscillator. They may be observed by applying a succession of simultaneous pressure and voltage (or current) clamps to the membrane. These stationary states of Teorell's membrane oscillator were first systematically examined by Franck (1963). He explained his observations by using a theory based on the fine pore model of the membrane (Schlögl 1964). In this approach the internal charge is assumed to be distributed homogeneously within the membrane pores. Such a condition can hold strictly only in membranes with effective pore diameters of 10 nm or less. The oscillations observed by Teorell and Franck were, however, excited in loosely granular membranes of effective pore sizes greater than 0.5 μm.

An alternative theory of the stationary states has been formulated by Kobatake & Fujita (1964).

PHILOSOPHICAL TRANSACTIONS OF THE ROYAL SOCIETY A MATHEMATICAL, PHYSICAL & ENGINEERING SCIENCES

It is based on a broad pore model of the membrane. These authors were concerned with interpreting some unpublished experiments of Tasaki carried out on glass sinters. In the theory of Kobatake & Fujita the internal structure of the membrane is described as an array of parallel cylindrical pores. The internal charge is regarded as localized on the pore walls and the pore diameters are sufficiently large for a diffuse electrical double layer to be formed in the pore space.

The treatment of Kobatake & Fujita makes use of an averaging procedure for the concentrations and ion fluxes over any cross-section in a pore. An alternative treatment of flow in capillaries, based on a more detailed hydrodynamic analysis has been discussed by Borsellino (1964). This theory may give a more complete picture of the local events which occur at the instant of transition between one steady state and another, but it is less suitable for describing the overall behaviour of the system throughout a wide range of fluxes and forces.

To date a critical and quantitative test of these stationary state theories has not been possible owing to the lack of a membrane of sufficiently well-characterized internal structure, although some observations have been made with single glass capillaries (Oliva 1967). Either a powder or a sinter membrane is very complex and its internal structure does not correspond with either of the theoretical models described above. This paper describes an investigation of the steady-state properties of a class of membranes with exceptionally well-defined pore structure and which are capable of oscillatory behaviour. These membranes are the Nuclepore filters manufactured by General Electric of America. They consist of a sheet of polycarbonate perforated by an array of discrete and nearly parallel cylindrical pores. The filters are available in a range of graded pore sizes. An electric charge is found to be associated with the polycarbonate surface when the filters are immersed in electrolyte solutions. Periodic and stationary state phenomena have been observed while filters of pore diameters of 0.5, 0.8, 1.0 and 2.0 μm were being used.

The paper begins by developing a theory of the stationary states on the basis of a broad pore membrane model similar to that used by Kobatake & Fujita (1964). The present treatment however differs from that of Kobatake & Fujita in that it uses the conjugated set of forces and fluxes recommended by Mikulecky & Caplan (1966). In addition, allowance is made for the concentration dependence of the surface charge within the pores, and for the presence of unstirred diffusion layers in the solutions adjacent to the membrane surface. The paper goes on to describe an experimental verification of the theory using Nuclepore filter membranes in a more refined apparatus than has been used by previous workers. It closes with a critical assessment of the correspondence between theory and experiment.

2. Theory

2.1. *Local flux equations*

The membrane will be regarded as an insoluble matrix penetrated by an array of parallel, right circular cylindrical pores. The pores are considered to have equal radii, and to be large compared to the mean free paths of the ions or molecules in the pore liquid. The pores run perpendicularly to the membrane faces which are separated by a distance large compared with the radii. An electric charge is associated with the membrane and pore surfaces. It gives rise to a diffuse region of electrical double layer within the solution filling the pores. The pore liquid is considered to be incompressible, isotropic and inelastic.

The properties of the whole membrane may be deduced from those of a typical pore which will now be considered. The analysis proceeds on the basis of the system shown in figure 1. The

pore liquid is in contact at the ends of the pore with the electrolyte solutions in compartments I and II. The solutions are assumed to be dilute and to be so well stirred that their concentrations are uniform outside the diffusion layers adjacent to the membrane surfaces. The volume of the solution in each compartment is sufficiently large that the effect of inter-mixing from one compartment to the other on the bulk concentrations is negligible. The concentrations of the solutions at the ends of the pore may differ somewhat from the bulk concentrations owing to the limited rates of transport in the solutions and depend on the vigour of the stirring and the fluxes in the

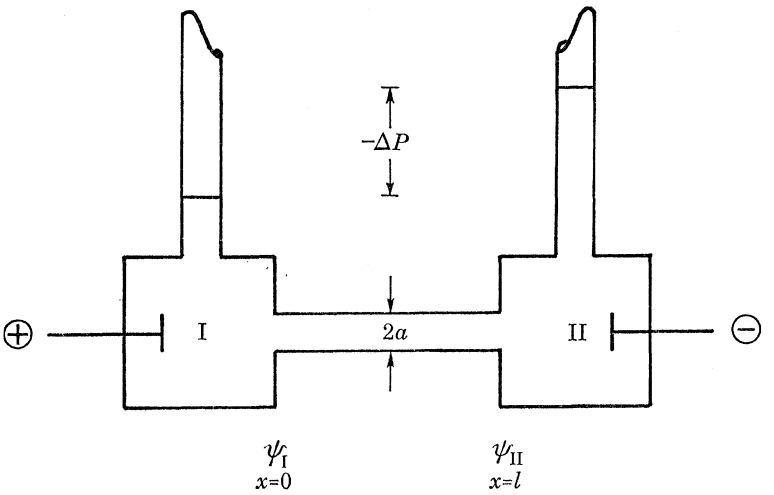

FIGURE 1. Solution reservoirs interconnected by a single capillary.

membrane. This polarization of concentration will be taken into account later. The solutions are of a single electrolyte in water and the more concentrated solution is in compartment II. The system is isothermal and no chemical reactions occur. The current-passing electrodes are so isolated that products of the electrode reactions cannot interfere with the system. Local mechanical equilibrium is assumed everywhere including within the pore media. A hydrostatic pressure difference ΔP may be set up as shown in figure 1.

De Groot & Mazur (1962) have shown that for a stationary state the dissipation function within a local volume element of pore space may be described by

$$T\dot{S} = -\sum_{\mathrm{k}=1}^{n} \boldsymbol{J}_{\mathrm{k}}(\mathrm{grad}\,\tilde{\mu}_{\mathrm{k}})_{\mathrm{T}} - \mathring{\boldsymbol{\Pi}}^{\mathrm{s}}:(\mathrm{d}\boldsymbol{v}/\mathrm{d}r), \tag{2.1.1}$$

where T represents temperature, $\dot{S}$ the local rate of entropy production per unit volume at any point within the membrane pore, $\boldsymbol{J}_{\mathrm{k}}$ the diffusional flux per unit area relative to the local centre of mass, $\boldsymbol{v}$ the barycentric velocity, $\tilde{\mu}_{\mathrm{k}}$ the electro-chemical potential of component k, $\mathring{\boldsymbol{\Pi}}^{\mathrm{s}}$ the symmetric pressure tensor and r the radial coordinate inside the pore. Specific quantities are used throughout, and $\mathrm{grad}\,\tilde{\mu}_{\mathrm{k}}$ in the pore is defined by

$$(\mathrm{grad}\,\tilde{\mu}_{\mathrm{k}})_{\mathrm{T}} = \left(\frac{\partial\tilde{\mu}_{\mathrm{k}}}{\partial x}\right)_{\mathrm{T}} = \left(\frac{\partial\mu_{\mathrm{k}}}{\partial x}\right)_{\mathrm{T,P}} + b_{\mathrm{k}}\left(\frac{\partial P}{\partial x}\right)_{\mathrm{T}} + e_{\mathrm{k}}\left(\frac{\partial\psi}{\partial x}\right)_{\mathrm{T}}, \tag{2.1.2}$$

where μ_{k} and e_{k} are respectively the chemical potential and electric charge per unit mass of species k; b_{k} is the partial specific volume of species k; P and ψ represent the local hydrostatic pressure and electric potential respectively.

Locally the fluxes are assumed to be linearly related to the forces, and also, in the local sense, the Onsager reciprocal relations hold. Thus from equation (2.1.1) we have

$$\boldsymbol{J}_k = -\sum_{j=1}^{n} L_{kj}(\partial\tilde{\mu}_j/\partial x); \tag{2.1.3}$$

here the L_{kj} are the local phenomenological coefficients in the barycentric frame. The electrolyte is made up of a single type of cation, subscript 1, and a single type of anion, subscript 2; water is given subscript 3. The electrolyte is assumed to be dilute so that the contribution to the local entropy production due to water diffusion relative to the centre of mass may be neglected. Hence

$$\boldsymbol{J}_3(\partial\tilde{\mu}_3/\partial x) = 0.$$

From the Gibbs–Duhem equation $\partial\tilde{\mu}_3/\partial x \neq 0$, hence this assumption implies

$$\boldsymbol{J}_3 = 0. \tag{2.1.4}$$

The equations of motion of the solution and of the water may be taken as identical (cf. Mikulecky & Caplan 1966; Kobatake & Fujita 1964).

Neglect of the coupling of ion and water fluxes in the barycentric frame leads to the conditions

$$L_{13} = L_{31} = L_{23} = L_{32} = 0.$$

It follows therefore from equation (2.1.3) that

$$L_{33} = 0.$$

It is also assumed that the diffusional flows relative to the local centre of mass arising from the contribution of pressure gradients to the chemical potential gradients are vanishingly small.

The membrane matrix is not included as a thermodynamic species, and the electrolyte solutions are assumed to be thermodynamically ideal. The electro-chemical potentials under these conditions are expressed by

$$\tilde{\mu}_k = \mu_k + e_k\psi, \tag{2.1.5}$$

and the chemical part μ_k by

$$\mu_k = \mu_k^0 + (RT/M_k)\ln\rho_k, \tag{2.1.6}$$

where ρ_k is the concentration of species k in mass per unit volume, M_k is the molecular weight of species k and R the universal gas constant.

The ion transport equations of the system are thus reduced to

$$\boldsymbol{J}_1 = -[L_{11}(\partial\tilde{\mu}_1/\partial x) + L_{12}(\partial\tilde{\mu}_2/\partial x)] \tag{2.1.7}$$

and

$$\boldsymbol{J}_2 = -[L_{21}(\partial\tilde{\mu}_1/\partial x) + L_{22}(\partial\tilde{\mu}_2/\partial x)]. \tag{2.1.8}$$

Experimentally it is much easier to measure a salt flux $\boldsymbol{J}_s$, and the electric current $\boldsymbol{i}$, rather than the individual ion fluxes $\boldsymbol{J}_k$. Equations (2.1.7) and (2.1.8) will now be transformed into expressions for the fluxes $\boldsymbol{J}_s$ and $\boldsymbol{i}$.

The ultimate aim is to evaluate the total flux through a pore which is assumed to be wide in comparison with the thickness of the electrical double layer at its wall. Under this assumption, the effect on the total ion content of the pore due to the net charge of the solution counter to the wall charge may be neglected and the condition of local electrical neutrality

$$e_1\rho_1 + e_2\rho_2 = 0 \tag{2.1.9}$$

then holds. Also, at every point, the relation

$$\rho_1 + \rho_2 = \rho_s \tag{2.1.10}$$

defines ρ_s, the local specific salt concentration. If ν_k is the number of ions of species k released by each molecule of electro-neutral salt, and z_k is the number of elementary electrostatic positive charges on each ion of species k, it follows that

$$z_1\nu_1 + z_2\nu_2 = 0. \tag{2.1.11}$$

Attention is restricted to electrolytes for which

$$\nu_2/z_1 = -\nu_1/z_2 = 1. \tag{2.1.12}$$

These conditions enable the following relation between the chemical potential gradients of the salt and the individual ions to be derived

$$\frac{M_s}{\nu}\left(\frac{\partial\mu_s}{\partial x}\right) = M_1\left(\frac{\partial\mu_1}{\partial x}\right) = M_2\left(\frac{\partial\mu_2}{\partial x}\right), \tag{2.1.13}$$

where $$\nu = \nu_1 + \nu_2.$$

If the ion flows are combined to form the salt flux J_s, defined by

$$J_s = \frac{M_s}{\nu}\left(\frac{J_1}{M_1} + \frac{J_2}{M_2}\right), \tag{2.1.14}$$

and the local electric current density is represented by

$$i = e_1 J_1 + e_2 J_2, \tag{2.1.15}$$

then the desired transformation may be carried out with the aid of equations (2.1.9) to (2.1.13) to give

$$J_s = -L_{ss}(\partial\mu_s/\partial x) - L_{si}(\partial\psi/\partial x), \tag{2.1.16}$$

$$i = -L_{is}(\partial\mu_s/\partial x) - L_{ii}(\partial\psi/\partial x), \tag{2.1.17}$$

where

$$L_{ss} = \left(\frac{M_s}{\nu}\right)^2\left(\frac{L_{11}}{M_1^2} + \frac{2L_{12}}{M_1M_2} + \frac{L_{22}}{M_2^2}\right), \tag{2.1.18}$$

$$L_{is} = L_{si} = \left(\frac{M_s}{\nu}\right)\left[\left(\frac{e_1}{M_1}\right)L_{11} + \left(\frac{e_1}{M_2} + \frac{e_2}{M_1}\right)L_{12} + \left(\frac{e_2}{M_2}\right)L_{22}\right], \tag{2.1.19}$$

$$L_{ii} = e_1^2 L_{11} + 2e_1e_2L_{12} + e_2^2L_{22}. \tag{2.1.20}$$

It is convenient at this stage to change the frame of reference of the fluxes J_s and i from the local centre of mass to the membrane matrix. This may be done by using the relations

$$(J_s)_c = J_s + \rho_s v, \tag{2.1.21}$$

$$(i)_c = i + (e_1\rho_1 + e_2\rho_2)\, v, \tag{2.1.22}$$

$$(J_3)_c = J_3 + \rho_3 v. \tag{2.1.23}$$

In equation (2.1.33) $(J_3)_c$ is the water flux relative to the membrane matrix. Recalling equation (2.1.4) and assuming the density of water ρ_3 to be unity equation (2.1.23) reduces to

$$(J_3)_c = v. \tag{2.1.24}$$

The barycentric velocity v has to be evaluated by considering the combined effects of pressure-driven and electro-osmotic flows in the pore. This problem was considered by Kobatake & Fujita (1964). They found the appropriate solution of the Navier–Stokes equation by assuming

streamline flow in the pore. This assumption is a good approximation in the case of a capillary whose length greatly exceeds its diameter and which is very broad compared with the thickness of the electrical double layer of ions at its wall. The absolute flow rates considered are so low that there is no danger of departure from laminar flow on this account. Kobatake & Fujita's solution is therefore adopted here: it is

$$v = \frac{r^2 - a^2}{4\eta}\left(\frac{\partial P}{\partial x}\right) - \frac{\epsilon(\phi - \phi_0)}{4\pi\eta}\left(\frac{\partial \psi}{\partial x}\right); \tag{2.1.25}$$

ϕ is the potential at a given point in the pore liquid measured radially with respect to the pore wall. The radius of the pore is a, and $\phi = \phi_0$ at $r = a$. The ratio of the pore length and pore radius is sufficiently large that both P and ψ are effectively independent of r except close to the periphery. The bulk dielectric constant of the solvent is ϵ and the coefficient of shear viscosity is η.

The effect of the electrical double layer close to the pore walls in producing an electro-osmotic plug flow of the solvent is very large. It may be noted that this effect is fully taken into consideration in equation (2.1.25).

2.2. *Macroscopic flux equations*

The macroscopic flux equations must now be obtained by integrating the local fluxes over the cross-section of the capillary. This may be done by using the relation

$$(\bar{J}_k)_c = \frac{\int_0^a (J_k)_c \, 2\pi r \, dr}{\int_0^a 2\pi r \, dr}. \tag{2.2.1}$$

When equation (2.1.25) is averaged in this way the following expression is obtained for the average barycentric velocity $\bar{v}$

$$\bar{v} = -\frac{a^2}{8\eta}\left(\frac{dP}{dx}\right) + \frac{\epsilon\phi_0}{4\pi\eta}\left(\frac{d\psi}{dx}\right) = (\bar{J}_3)_c, \tag{2.2.2}$$

where ϕ_0 is the potential at the capillary wall. ϕ_0 can be expressed in terms of κ, the Debye–Hückel reciprocal length, defined by

$$\kappa^2 = 4\pi F^2 \nu_1 \nu_2 \nu \rho_s / (\epsilon R T M_s), \tag{2.2.3}$$

where F is Faraday's constant. Provided $\kappa a \gg 1$ the relation between ϕ_0 and κ is

$$\phi_0 = 4\pi\sigma/\epsilon\kappa, \tag{2.2.4}$$

where σ is the surface charge density on the pore walls. Equations (2.2.2) and (2.2.4) may now be combined to give

$$\bar{v} = -\frac{a^2}{8\eta}\left(\frac{dP}{dx}\right) + \frac{\sigma}{\kappa\eta}\left(\frac{d\psi}{dx}\right). \tag{2.2.5}$$

The averaged salt flux has to be obtained by integrating equation (2.1.21). Strictly this requires the average salt concentration $\bar{\rho}_s$ to be evaluated. Because the area of the region close to the capillary walls where the concentrations are perturbed by the electrical double layer is but a very small fraction of the total cross-section area of the capillary the effect of these concentration perturbations on the average concentration over the whole cross-section may be neglected. The averaged version of the second term on the right-hand side of equation (2.1.21) may therefore be taken as $\rho_s \bar{v}$. The averaged version of the first term on the right-hand side of equation (2.1.21) is obtained by averaging equation (2.1.16) because it has been assumed that

the averaged concentration differs negligibly from the axial concentration. It is consistent to assume also that the coefficients L_{ss} and L_{si} related to the axial concentration may also be used in the averaged equations. Furthermore, the assumption regarding ρ_s requires that $d\mu_s/dx$ be independent of the radial coordinate. The assumption of streamline electro-osmotic flow in wide pores made above requires that $d\psi/dx$ is also independent of r. Thus the averaged value of the salt flux becomes simply

$$(\bar{J}_s)_c = -L_{ss}(d\mu_s/dx) - L_{si}(d\psi/dx) + \rho_s \bar{v}. \tag{2.2.6}$$

The assumptions made above are equivalent to neglecting any additional flux in the electrical double layer in comparison with the total salt flux in the capillary.

Most of the principles used in evaluating the averaged salt flux apply also to the integration of equations (2.1.17) and (2.1.22) for the averaged current density in the pore. Thus in equation (2.1.17) the coefficients L_{is} and L_{ii} are independent of r as are also the two driving forces. The second term on the right-hand side of equation (2.1.22) is concerned with the streaming current. The assumption made in equation (2.1.9) when applied to equation (2.1.22) amounts to ignoring the contribution of the streaming current to the total current.

The validity of this assumption in the present context may be seen as follows, in the case where $\rho_I = \rho_{II}$ the streaming current density over the membrane surface I_s may be written

$$I_s = \pi a^2 \sigma N \Delta P / l\eta\kappa. \tag{2.2.7}$$

Here N is the number of pores per unit area of membrane and ΔP the hydrostatic pressure difference across the membrane thickness l. Substitution of experimental values into this equation has shown that I_s never exceeded $0.2\,\mathrm{A\,m^{-2}}$. The experimental current densities were always greater than $100\,\mathrm{A\,m^{-2}}$. Thus it is clear that no serious error arises from neglecting the streaming current.

The expression for the averaged electric current density therefore derives directly from equation (2.1.17) which becomes

$$(\bar{i})_c = -L_{is}(d\mu_s/dx) - L_{ii}(d\psi/dx). \tag{2.2.8}$$

It can be shown that equations (2.2.6) and (2.2.8) are equivalent to the Nernst–Planck flux equations for the ions in the capillary with allowance being made for the average convection velocity $\bar{v}$ (Teorell 1951). The electro-neutrality condition, equation (2.1.9) can also be expressed as

$$\rho_I/(M_1\nu_1) = \rho_2/(M_2\nu_2). \tag{2.2.9}$$

When this is used to eliminate ρ_2 from equation (2.1.10) and the result differentiated one may obtain

$$\frac{1}{\rho_1}\left(\frac{d\rho_1}{dx}\right) = \frac{1}{\rho_s}\left(\frac{d\rho_s}{dx}\right). \tag{2.2.10}$$

By differentiating equation (2.1.6) and combining the result with equation (2.1.13) and (2.2.10) the chemical potential gradient $(d\mu_s/dx)$ is found to be given by

$$\frac{d\mu_s}{dx} = \frac{\nu RT}{M_s\rho_s}\left(\frac{d\rho_s}{dx}\right). \tag{2.2.11}$$

This expression may be substituted into equations (2.2.6) and (2.2.8) to give

$$(\bar{J}_s)_c = -\frac{L_{ss}\nu RT}{M_s\rho_s}\left(\frac{d\rho_s}{dx}\right) - L_{si}\left(\frac{d\psi}{dx}\right) + \rho_s\bar{v}, \tag{2.2.12}$$

$$(\bar{i})_c = -\frac{L_{is}\nu RT}{M_s\rho_s}\left(\frac{d\rho_s}{dx}\right) - L_{ii}\left(\frac{d\psi}{dx}\right). \tag{2.2.13}$$

PHILOSOPHICAL TRANSACTIONS OF THE ROYAL SOCIETY A MATHEMATICAL, PHYSICAL & ENGINEERING SCIENCES

The corrected Nernst–Planck equations, when expressed in terms of molar fluxes $\boldsymbol{j}_k$ and molar concentrations c_k, are

$$\boldsymbol{j}_1 = -D_1(\mathrm{d}c_1/\mathrm{d}x) - Fz_1c_1u_1(\mathrm{d}\psi/\mathrm{d}x) + c_1\bar{\boldsymbol{v}}, \tag{2.2.14}$$

$$\boldsymbol{j}_2 = -D_2(\mathrm{d}c_2/\mathrm{d}x) - Fz_2c_2u_2(\mathrm{d}\psi/\mathrm{d}x) + c_2\bar{\boldsymbol{v}}, \tag{2.2.15}$$

where D_k is the diffusion coefficient and u_k the absolute mobility of ionic species k.

From equation (2.1.14) the molar salt flux $\boldsymbol{j}_s$ may be defined by

$$\boldsymbol{J}_s/M_s = (\boldsymbol{j}_1+\boldsymbol{j}_2)/\nu = \boldsymbol{j}_s, \tag{2.2.16}$$

whereas the electric current density $\boldsymbol{i}$, in terms of molar fluxes, is given by

$$\boldsymbol{i} = F(z_1\boldsymbol{j}_1+z_2\boldsymbol{j}_2); \tag{2.2.17}$$

remembering that electro-neutrality requires

$$c_1/\nu_1 = c_2/\nu_2 = c_s = \rho_s/M_s, \tag{2.2.18}$$

and combining equations (2.2.14), (2.2.15) and (2.1.11) with (2.2.16) or (2.2.17) we obtain for the fluxes $\boldsymbol{J}_s$ and $\boldsymbol{i}$

$$\boldsymbol{J}_s = -\frac{1}{\nu}(\nu_1D_1+\nu_2D_2)\left(\frac{\mathrm{d}\rho_s}{\mathrm{d}x}\right) - \frac{\nu_1\nu_2F}{\nu}(u_1-u_2)\,\rho_s\left(\frac{\mathrm{d}\psi}{\mathrm{d}x}\right) + \rho_s\bar{\boldsymbol{v}}, \tag{2.2.19}$$

$$\boldsymbol{i} = -\frac{\nu_1\nu_2F}{M_s}(D_1-D_2)\left(\frac{\mathrm{d}\rho_s}{\mathrm{d}x}\right) - \frac{\nu_1\nu_2F^2}{M_s}(\nu_2u_1+\nu_1u_2)\,\rho_s\left(\frac{\mathrm{d}\psi}{\mathrm{d}x}\right). \tag{2.2.20}$$

The comparison of equation (2.2.12) with (2.2.19) and of (2.2.13) with (2.2.20) shows that the averaged salt flux and current densities in a capillary have the same form as the extended Nernst–Planck expressions for $\boldsymbol{J}_s$ and $\boldsymbol{i}$. This permits the L_{1s} coefficients to be identified in terms of the D_k and u_k. The approximations and assumptions which have been made in the preceding derivation are required to make the extended Nernst–Planck equations consistent with the thermodynamics of irreversible processes. It may be noted that in order to preserve strict Onsager reciprocity between the coefficients L_{is} and L_{si} the Nernst–Einstein relation should apply between D_k and u_kRT at all concentrations.

In order to achieve a compact notation in the following sections four parameters are defined by

$$D = L_{ss}\nu RT/M_s\rho_s = (\nu_1D_1+\nu_2D_2)/\nu, \tag{2.2.21}$$

$$\Lambda = L_{ii}/\rho_s = \nu_1\nu_2F^2(\nu_2u_1+\nu_1u_2)/M_s, \tag{2.2.22}$$

$$D' = -L_{si}/\rho_s = -\nu_1\nu_2F(u_1-u_2)/\nu, \tag{2.2.23}$$

$$\Lambda' = L_{is}\nu RT/M_s\rho_s = \nu_1\nu_2F(D_1-D_2)/M_s. \tag{2.2.24}$$

2.3. *Integration of the macroscopic flux equations*

Equations (2.2.5), (2.2.12) and (2.2.13) must be integrated across the membrane under the appropriate boundary conditions, and in the stationary state. In practice it was found that substantial unstirred diffusion layers always existed adjacent to the membrane surfaces. The electrolyte concentrations at the membrane surfaces ρ_I^m and ρ_{II}^m were therefore not the same as the bulk concentrations ρ_I and ρ_{II}. The following boundary conditions are therefore imposed on the integrations

$$\left.\begin{aligned}\rho_s &= \rho_I^m, \quad P = P_I, \quad \psi = \psi_I \quad \text{at} \quad x = 0,\\ \rho_s &= \rho_{II}^m, \quad P = P_{II}, \quad \psi = \psi_{II} \quad \text{at} \quad x = l.\end{aligned}\right\} \tag{2.3.1}$$

PHILOSOPHICAL TRANSACTIONS OF THE ROYAL SOCIETY A MATHEMATICAL, PHYSICAL & ENGINEERING SCIENCES
PHILOSOPHICAL TRANSACTIONS OF THE ROYAL SOCIETY A MATHEMATICAL, PHYSICAL & ENGINEERING SCIENCES

The conditions of steady-state flow can be expressed as

$$\frac{\mathrm{d}(J_s)_c}{\mathrm{d}x} = \frac{\mathrm{d}(i)_c}{\mathrm{d}x} = \frac{\mathrm{d}\bar{v}}{\mathrm{d}x} = 0. \tag{2.3.2}$$

From equations (2.2.12) and (2.2.13), together with the definitions of equations (2.2.21) to (2.2.24), the following may be obtained:

$$J_s = -D(\mathrm{d}\rho_s/\mathrm{d}x) + D'\rho_s(\mathrm{d}\psi/\mathrm{d}x) + \rho_s \bar{v}, \tag{2.3.3}$$

$$i = -\Lambda'(\mathrm{d}\rho_s/\mathrm{d}x) - \rho_s \Lambda(\mathrm{d}\psi/\mathrm{d}x). \tag{2.3.4}$$

The identification of the L_{is} coefficients through equations (2.2.19) and (2.2.20) makes it appropriate to use the symbols J_s and i in place of $(\bar{J}_s)_c$ and $(\bar{i})_c$.

Equations (2.3.3) and (2.3.4) are now used in order to integrate equation (2.2.5). Under the boundary conditions (2.3.1) the volume flow equation (2.2.5) may be rewritten in the integral form, provided $\rho_I^m \neq \rho_{II}^m$,

$$\bar{v}\int_0^l \mathrm{d}x = -\frac{a^2}{8\eta}\int_{P_I}^{P_{II}} \mathrm{d}P + \int_{\rho_I^m}^{\rho_{II}^m} \frac{\sigma}{\kappa\eta}\left(\frac{\mathrm{d}\psi}{\mathrm{d}x}\right)\left(\frac{\mathrm{d}x}{\mathrm{d}\rho_s}\right)\mathrm{d}\rho_s. \tag{2.3.5}$$

$\mathrm{d}\psi/\mathrm{d}x$ may be eliminated from equations (2.3.3) and (2.3.4) and the resulting equation solved for $\mathrm{d}\rho_s/\mathrm{d}x$ to give

$$\frac{\mathrm{d}\rho_s}{\mathrm{d}x} = -\left(J_s + \frac{D'i}{\Lambda}\right)\frac{1}{D_s} + \frac{\rho_s \bar{v}}{D_s}, \tag{2.3.6}$$

where the Nernst limiting diffusion coefficient of the salt D_s is given by

$$D_s = D(1 + D'\Lambda'/D\Lambda) = (z_1u_1D_2 - z_2u_2D_1)/(z_1u_1 - z_2u_2). \tag{2.3.7}$$

It is convenient to define a combination of the steady-state fluxes of salt and current α by

$$\alpha = -(J_s + D'i/\Lambda). \tag{2.3.8}$$

Equations (2.3.3) and (2.3.4) are now solved for $\mathrm{d}\psi/\mathrm{d}x$ and the result divided by equation (2.3.6) to give

$$\left(\frac{\mathrm{d}\psi}{\mathrm{d}x}\right)\Big/\left(\frac{\mathrm{d}\rho_s}{\mathrm{d}x}\right) = -\frac{D_s[i + \Lambda'(\alpha + \rho_s\bar{v})/D_s]}{\rho_s\Lambda(\alpha + \rho_s\bar{v})}. \tag{2.3.9}$$

Electro-osmotic experiments showed that in Nuclepore membranes the surface charge had the following dependence upon electrolyte concentration

$$\sigma = K\rho_s^{\frac{1}{2}}, \tag{2.3.10}$$

where K is a constant, independent of concentration. Such a functional dependence may also have a theoretical basis at low concentration where the surface charge results from ion adsorption (Benton & Elton 1958). It may therefore hold also in other non-ionogenic membranes.

From equation (2.2.3) the concentration dependence of the Debye–Hückel reciprocal length may be fully expressed by

$$\kappa = \beta\rho_s^{\frac{1}{2}}, \tag{2.3.11}$$

where

$$\beta = (4\pi F^2\nu_1\nu_2\nu/\epsilon RTM_s)^{\frac{1}{2}}. \tag{2.3.12}$$

Hence, on combining equations (2.3.10) and (2.3.11), one finds

$$\frac{\sigma}{\kappa\eta} = \frac{K}{\beta\eta}\left(\frac{1}{\rho_s}\right)^{\frac{1}{6}}. \tag{2.3.13}$$

When equations (2.3.9) and (2.3.13) are substituted into (2.3.5) it can be written in the integral form

$$\bar{\boldsymbol{v}}\int_0^l \mathrm{d}x = -\frac{a^2}{8\eta}\int_{P_\mathrm{I}}^{P_\mathrm{II}}\mathrm{d}P - \frac{K\Lambda'}{\beta\eta\Lambda}\int_{\rho_\mathrm{I}^m}^{\rho_\mathrm{II}^m}\frac{\mathrm{d}\rho_\mathrm{s}}{\rho_\mathrm{s}^{\frac{7}{6}}} - \frac{KD_\mathrm{s}\boldsymbol{i}}{\beta\eta\Lambda\boldsymbol{\alpha}}\int_{\rho_\mathrm{I}^m}^{\rho_\mathrm{II}^m}\frac{\mathrm{d}\rho_\mathrm{s}}{\rho_\mathrm{s}^{\frac{7}{6}}(1+\rho_\mathrm{s}\bar{\boldsymbol{v}}/\boldsymbol{\alpha})}. \tag{2.3.14}$$

Integration of equation (2.3.14) gives finally

$$\bar{\boldsymbol{v}}l = \frac{a^2\Delta P}{8\eta} - \frac{6K}{\beta\eta\Lambda}\left[\left(\frac{1}{\rho_\mathrm{I}^m}\right)^{\frac{1}{6}} - \left(\frac{1}{\rho_\mathrm{II}^m}\right)^{\frac{1}{6}}\right]\left(\Lambda' + \frac{D_\mathrm{s}\boldsymbol{i}}{\boldsymbol{\alpha}}\right) - \frac{KD_\mathrm{s}\boldsymbol{i}}{\beta\eta\Lambda\boldsymbol{\alpha}}\Gamma, \tag{2.3.15}$$

where

$$\Delta P = P_\mathrm{I} - P_\mathrm{II}, \tag{2.3.16}$$

$$\Gamma = \left(\frac{\bar{\boldsymbol{v}}}{\boldsymbol{\alpha}}\right)^{\frac{1}{6}}\left[\arctan(2t-\sqrt{3}) + \arctan(2t+\sqrt{3}) + 2\arctan t + \frac{\sqrt{3}}{2}\ln\left(\frac{t^2+\sqrt{(3)}\,t+1}{t^2-\sqrt{(3)}\,t+1}\right)\right]_{t_\mathrm{I}}^{t_\mathrm{II}} \tag{2.3.17}$$

with t_I and t_II given by

$$t_\mathrm{I} = \left(\frac{\boldsymbol{\alpha}}{\bar{\boldsymbol{v}}\rho_\mathrm{I}}\right)^{\frac{1}{6}} \quad \text{and} \quad t_\mathrm{II} = \left(\frac{\boldsymbol{\alpha}}{\bar{\boldsymbol{v}}\rho_\mathrm{II}}\right)^{\frac{1}{6}}. \tag{2.3.18}$$

In the case of a membrane with ionizable groups chemically bound to the polymer matrix forming the pore walls the surface charge density will be virtually independent of the concentration of the solution in the pores, except at very high concentrations. If the surface charge has a constant density $\bar{\sigma}$ equation (2.3.14) must be replaced by

$$\bar{\boldsymbol{v}}\int_0^l \mathrm{d}x = -\frac{a^2}{8\eta}\int_{P_\mathrm{I}}^{P_\mathrm{II}}\mathrm{d}P - \frac{\bar{\sigma}\Lambda'}{\beta\eta\Lambda}\int_{\rho_\mathrm{I}^m}^{\rho_\mathrm{II}^m}\frac{\mathrm{d}\rho_\mathrm{s}}{\rho_\mathrm{s}^{\frac{3}{2}}} - \frac{D_\mathrm{s}\bar{\sigma}\boldsymbol{i}}{\beta\eta\Lambda\boldsymbol{\alpha}}\int_{\rho_\mathrm{I}^m}^{\rho_\mathrm{II}^m}\frac{\mathrm{d}\rho_\mathrm{s}}{\rho_\mathrm{s}^{\frac{3}{2}}(1+\rho_\mathrm{s}\bar{\boldsymbol{v}}/\boldsymbol{\alpha})}. \tag{2.3.19}$$

On integration equation (2.3.19) becomes

$$\bar{\boldsymbol{v}}l = \frac{a^2\Delta P}{8\eta} - \frac{2\bar{\sigma}}{\beta\eta\Lambda}\left[\left(\frac{1}{\rho_\mathrm{I}^m}\right)^{\frac{1}{2}} - \left(\frac{1}{\rho_\mathrm{II}^m}\right)^{\frac{1}{2}}\right]\left(\Lambda' + \frac{D_\mathrm{s}\boldsymbol{i}}{\boldsymbol{\alpha}}\right) - \frac{2\bar{\sigma}D_\mathrm{s}i}{\beta\eta\Lambda\boldsymbol{\alpha}}\left(\frac{\bar{\boldsymbol{v}}}{\boldsymbol{\alpha}}\right)^{\frac{1}{2}}\left(\arctan\frac{1}{t_\mathrm{I}^3} - \arctan\frac{1}{t_\mathrm{II}^3}\right). \tag{2.3.20}$$

This equation will not be used here because it is not appropriate for Nuclepore membranes. It would apply to membranes formed from a polyelectrolyte matrix.

Once the expression for $\bar{\boldsymbol{v}}$ has been obtained the relations between the other fluxes and forces can be derived in terms of $\bar{\boldsymbol{v}}$ in a straightforward way.

From equations (2.3.6) and (2.3.8) it follows that

$$\boldsymbol{\alpha} = D_\mathrm{s}(\mathrm{d}\rho_\mathrm{s}/\mathrm{d}x) - \rho_\mathrm{s}\bar{\boldsymbol{v}}. \tag{2.3.21}$$

The solution to this equation under the given boundary conditions is well known and can be written

$$\boldsymbol{\alpha} = \frac{\bar{\boldsymbol{v}}[\rho_\mathrm{II}^m - \rho_\mathrm{I}^m\exp(\bar{\boldsymbol{v}}l/D_\mathrm{s})]}{\exp(\bar{\boldsymbol{v}}l/D_\mathrm{s}) - 1}. \tag{2.3.22}$$

Defining a membrane potential difference by

$$\Delta\psi = \psi_\mathrm{I} - \psi_\mathrm{II} \tag{2.3.23}$$

it is evident that

$$\Delta\psi = \int_{\rho_\mathrm{II}^m}^{\rho_\mathrm{I}^m}\left(\frac{\mathrm{d}\psi}{\mathrm{d}x}\right)\left(\frac{\mathrm{d}x}{\mathrm{d}\rho_\mathrm{s}}\right)\mathrm{d}\rho_\mathrm{s}. \tag{2.3.24}$$

Substitution of $(\mathrm{d}\psi/\mathrm{d}x)\times(\mathrm{d}x/\mathrm{d}\rho_\mathrm{s})$ from equation (2.3.9) into equation (2.3.24) and integration yields

$$\Delta\psi = -\frac{\Lambda'}{\Lambda}\ln\left(\frac{\rho_\mathrm{I}^m}{\rho_\mathrm{II}^m}\right) - \frac{D_\mathrm{s}\boldsymbol{i}}{\Lambda\boldsymbol{\alpha}}\left[\frac{\bar{\boldsymbol{v}}l}{D_\mathrm{s}} + \ln\left(\frac{\rho_\mathrm{I}^m}{\rho_\mathrm{II}^m}\right)\right]. \tag{2.3.25}$$

PHILOSOPHICAL TRANSACTIONS OF THE ROYAL SOCIETY A MATHEMATICAL, PHYSICAL & ENGINEERING SCIENCES

It should be noticed that the second term on the right-hand side in equation (2.3.25) becomes zero when $\boldsymbol{i}$ is zero. The first term on the right, $-(\Lambda'/\Lambda)\ln(\rho_{\mathrm{I}}^m/\rho_{\mathrm{II}}^m)$, therefore represents the liquid junction potential $\Delta\psi_{\mathrm{d}}$ between the interfacial solutions. This is readily verified by substituting for Λ and Λ' from equations (2.2.22) and (2.2.24).

Similarly, equation (2.3.15) becomes, when $\boldsymbol{i}$ and $\bar{v}$ are set at zero,

$$\Delta P_0 = \frac{48K\Lambda'}{\beta a^2\Lambda}\left[\left(\frac{1}{\rho_{\mathrm{I}}^m}\right)^{\frac{1}{6}} - \left(\frac{1}{\rho_{\mathrm{II}}^m}\right)^{\frac{1}{6}}\right]. \tag{2.3.26}$$

Here ΔP_0 is the osmotic pseudo-equilibrium pressure or anomalous osmotic pressure which would be generated across such a broad pore membrane.

In the case of constant $\bar{\sigma}$ equation (2.3.20) gives, when $\boldsymbol{i}$ and $\bar{v}$ are zero,

$$\Delta P_0 = \frac{16\bar{\sigma}\Lambda'}{\beta a^2\Lambda}\left[\left(\frac{1}{\rho_{\mathrm{I}}^m}\right)^{\frac{1}{2}} - \left(\frac{1}{\rho_{\mathrm{II}}^m}\right)^{\frac{1}{2}}\right]. \tag{2.3.27}$$

The integral resistance of the membrane per unit area of pores r_{m} can be defined by $(\Delta\psi - \Delta\psi_{\mathrm{j}})/\boldsymbol{i}$. By substituting $\boldsymbol{\alpha}$ from equation (2.3.22) into (2.3.25) it is found that

$$r_{\mathrm{m}} = \frac{l}{\Lambda}\left\{\frac{[\bar{v}l/D_{\mathrm{s}} + \ln(\rho_{\mathrm{I}}^m/\rho_{\mathrm{II}}^m)]\,[1-\exp(\bar{v}l/D_{\mathrm{s}})]}{(\bar{v}l/D_{\mathrm{s}})\,[\rho_{\mathrm{II}}^m - \rho_{\mathrm{I}}^m\exp(\bar{v}l/D_{\mathrm{s}})]}\right\}. \tag{2.3.28}$$

This expression has the same form as that given by Franck (1963) for the resistance of a fine pore membrane but in his treatment $\bar{v}$ bears a different relation to the membrane parameters.

The set of equations (2.3.8), (2.3.15), (2.3.22) and (2.3.25) together with their ancillaries permit the fluxes $\bar{v}$, $\boldsymbol{J}_{\mathrm{s}}$ and $\boldsymbol{i}$ and also the forces ΔP and $\Delta\psi$ to be calculated provided any two of these are fixed together with ρ_{I}^m and ρ_{II}^m, the boundary concentrations.

The fluxes so obtained are flux densities in the pores. They are readily converted to membrane flux densities V_{m}, J_{m} and I_{m} by multiplying $\bar{v}$, $\boldsymbol{J}_{\mathrm{s}}$ and $\boldsymbol{i}$ by $(\pi a^2 N)$ where N is the number of pores per unit area of membrane surface. The integral resistance per unit area of the membrane R_{m} is obtained by dividing r_{m} by $(\pi a^2 N)$.

2.4. *The influence of stagnant solution layers*

In experiments with thin broad pore membranes it is impossible to stir the bulk phases very vigorously without incurring the danger of exaggerating pore end effects and of pulsing solutions right through the membrane. In consequence the likelihood of serious modification of the fluxes due to the presence of imperfectly mixed layers close to the membrane is greater than it would be in experiments with less hydrodynamically permeable membranes. Furthermore the expectation of considerable volume fluxes in the membrane complicates the usual methods chosen to allow for these layers.

In order to include the effects of restricted stirring in the theoretical treatment the Nernst stagnant layer model has been adopted here. It is assumed that the membrane is bounded by completely non-stirred layers of solution of thickness δ. Beyond these layers mixing is complete and the solutions have constant concentrations ρ_{I} and ρ_{II}.

The object is to express ρ_{I}^m and ρ_{II}^m in terms of ρ_{I}, ρ_{II} and δ in order to use the membrane flux equations. The achievement of this objective is based on the requirement that in the steady state the fluxes across the films and the membrane must all be equal.

It is assumed that the fluxes in the stagnant layers are caused by diffusion, ionic conduction

and the volume flux through the membrane. Zero pressure gradient in the films is assumed and transport is regarded as uniformly spread over the films and only uni-directional.

This assumption disregards the fact that the membrane surface is made up of a random distribution of separate pores. The assumption is justified by the fact that the mean distance between pore centres is typically in the region of 5 μm in the membranes studied in this work, whereas the stagnant layers were more than 100 μm thick.

The fluid in the solution films adjacent to the membrane surfaces must, on the assumptions made, be homogeneous in the plane normal to the axial coordinates. The idealizations of properties made about the film fluids are just as for the pore fluid. The fluxes through the membrane being equated to the fluxes through the stagnant films, the fluxes passing through unit area of a film can be written as

$$J_m = -D(d\rho_s/dx) + D'\rho_s(d\psi/dx) + \rho_s V_m, \tag{2.4.1}$$

$$I_m = -\Lambda'(d\rho_s/dx) - \Lambda\rho_s(d\psi/dx). \tag{2.4.2}$$

Elimination of $(d\psi/dx)$ from equations (2.4.1) and (2.4.2) followed by differentiation with respect to x gives, in the steady state,

$$\frac{d^2\rho_s}{dx^2} - \frac{V_m}{D_s}\frac{d\rho_s}{dx} = 0. \tag{2.4.3}$$

The solution of equation (2.4.3) is

$$\rho_s = G\exp(V_m x/D_s) + H, \tag{2.4.4}$$

where G and H are constants determined by the boundary concentrations.

Substitution of equation (2.4.4) into (2.4.1) combined with (2.4.2) yields

$$J_m = -I_m D'/\Lambda + V_m H \tag{2.4.5}$$

which, on comparison with equation (2.3.8) and (2.3.22), shows that

$$H = \frac{\alpha}{\bar{\nu}} = \frac{\rho_I^m \exp(\bar{\nu}l/D_s) - \rho_{II}^m}{\exp(\bar{\nu}l/D_s) - 1}. \tag{2.4.6}$$

Integration of the unstirred film equations, using as boundary conditions

$$\left.\begin{array}{llll} x = -\delta, & \rho_s = \rho_I; & x = 0, & \rho_s = \rho_I^m, \\ x = l, & \rho_s = \rho_{II}^m; & x = l+\delta, & \rho_s = \rho_{II}, \end{array}\right\} \tag{2.4.7}$$

therefore yields from equations (2.4.4) and (2.4.6)

$$\rho_I^m = \frac{\rho_I \exp(V_m\delta/D_s)\{\exp[(V_m\delta + \bar{\nu}l)/D_s] - 1\} + \rho_{II}[\exp(V_m\delta/D_s) - 1]}{\exp[(2V_m\delta + \bar{\nu}l)/D_s] - 1}, \tag{2.4.8}$$

$$\rho_{II}^m = \frac{\rho_{II}[\exp(\bar{\nu}l/D_s) - 1] + \rho_I^m \exp(\bar{\nu}l/D_s)[\exp(V_m\delta/D_s) - 1]}{\exp[(V_m\delta + \bar{\nu}l)/D_s] - 1}. \tag{2.4.9}$$

The values of ρ_I^m and ρ_{II}^m are thereby related to ρ_I and ρ_{II} and these two equations are used together with the membrane flux equations in subsequent calculations.

The electrical resistance of the unstirred film on side I is given by

$$R_{fI} = \frac{1}{\Lambda}\int_0^\delta \frac{dx}{\rho_s} = \frac{1}{\Lambda}\int_0^\delta \frac{dx}{G_I\exp(V_m x/D_s) + H}, \tag{2.4.10}$$

and analogously on side II. Integration of equation (2.4.10) gives

$$R_{\mathrm{fI}} = \frac{1}{AH}\left\{\delta - \frac{D_{\mathrm{s}}}{V_{\mathrm{m}}}\ln\left[\frac{G_{\mathrm{I}}\exp\left(V_{\mathrm{m}}\delta/D_{\mathrm{s}}\right)+H}{G_{\mathrm{I}}+H}\right]\right\} \tag{2.4.11}$$

where, on side I,

$$G_{\mathrm{I}} = \rho_{\mathrm{I}} - H \tag{2.4.12}$$

on the concentrated side II the expression for R_{fII} is analogous to equation (2.4.11) but with G_{II} given by

$$G_{\mathrm{II}} = (\rho_{\mathrm{II}} - H)/\exp\left(V_{\mathrm{m}}\,\delta/D_{\mathrm{s}}\right). \tag{2.4.13}$$

2.5. *Computations based on the theory*

In order to test the theory and also to use it for prediction it is necessary to be able to calculate the expected fluxes and forces under known external constraints through a membrane with

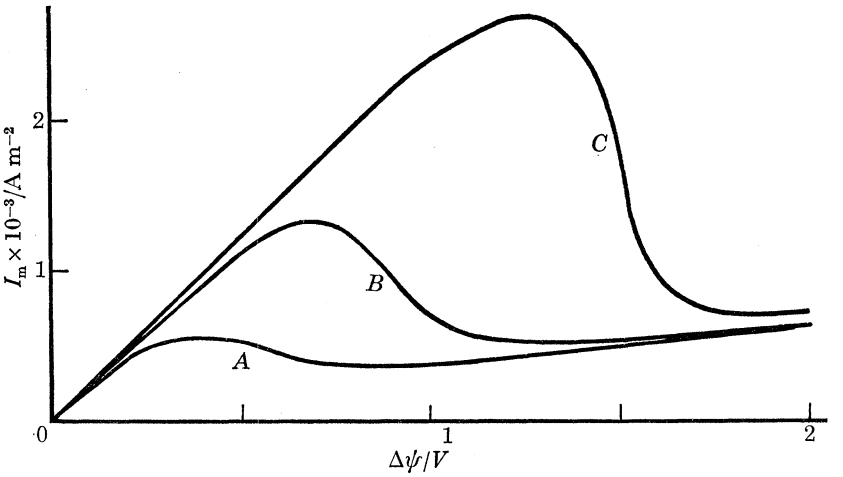

FIGURE 2. Plot of current density I_{m} against potential difference $\Delta\psi$ computed at three pressures ΔP. Curve A, $\Delta P = -196$ Pa; curve B, $\Delta P = -392$ Pa; curve C, $\Delta P = -687$ Pa.

certain known physical properties. In this section the methods of calculation are considered and in the next the appropriate physical properties and external parameters are identified.

The principal problem in calculation arises from the intimate dependence of the other fluxes and of the boundary concentrations on the volume flux, while the volume flux is normally an unconstrained variable under experimental conditions. The most convenient calculation procedure proved to be the following.

A value was selected for the volume flux $\bar{v}$ which lay within the expected range (after a little experience there was no difficulty in making a suitable choice). This value of $\bar{v}$, together with the bulk concentrations ρ_{I} and ρ_{II}, were substituted into equations (2.4.8) and (2.4.9) and the boundary concentrations ρ_{I}^{m} and ρ_{II}^{m} were obtained. The flux parameter $\boldsymbol{\alpha}$ was then calculated from equation (2.3.22).

The electric current density $\boldsymbol{i}$ which corresponded with the chosen volume flux $\bar{v}$ under the known pressure differential was obtained from equation (2.3.14) by numerical integration (McKeeman & Tesler 1963) because this was more convenient for computation than the explicit integral in equation (2.3.15).

The salt flux J_{s} followed from $\boldsymbol{\alpha}$, $\boldsymbol{i}$ and equation (2.3.8) and the membrane potential difference $\Delta\psi$ from $\boldsymbol{\alpha}$, $\boldsymbol{i}$ and equation (2.3.25). The membrane resistance r_{m} was calculated directly from

PHILOSOPHICAL TRANSACTIONS OF THE ROYAL SOCIETY A MATHEMATICAL, PHYSICAL & ENGINEERING SCIENCES

equation (2.3.28). The fluxes and currents per unit area of membrane were obtained from $\bar{\boldsymbol{v}}$, $\boldsymbol{J}_s$ and $\boldsymbol{i}$ by multiplication by the effective pore area per unit area of membrane.

The resistances of the stagnant layers at the membrane/solution interfaces were evaluated from equations (2.4.6) and (2.4.11).

The calculations were repeated for a series of selected values of the volume flux until enough values of the membrane current density I_m and potential difference $\Delta\psi$ had been obtained to construct a current–voltage plot. A typical example at three values of ΔP is shown in figure 2. The selected values of $\bar{v}$ at which I_m and $\Delta\psi$ were evaluated were especially closely spaced in the regions of the maximum and minimum in the current–voltage curve.

The authors' calculations were performed on the Aberdeen University I.C.L. Systems 4/50 computer.

2.6. *Membrane and system parameters*

In a typical steady state configuration a membrane of known properties separates two electrolyte solutions of known bulk concentrations. The pressure difference across the membrane and the electric current through it are also controlled by the experimenter.

The transport constants D_s, Λ, D' and Λ' of the electrolyte solutions may be obtained from published values of the appropriate conductivities and transport numbers (see, for example, Harned & Owen 1960). The conductivity coefficient Λ is related to the ordinary equivalent conductivity Λ_{eq} by

$$\Lambda = z_1 z_2 \Lambda_{eq}/1000 M_s. \tag{2.6.1}$$

The mean values of the equivalent conductivity and transport numbers appropriate to each pair of solution concentrations are obtained by graphical integration of the published data according to the relation

$$\bar{Q} = \int_{\rho_I}^{\rho_{II}} Q \, \mathrm{d}\rho_s/(\rho_{II}-\rho_I), \tag{2.6.2}$$

where Q is the parameter to be averaged.

Recalling that it was necessary to adopt the Nernst–Einstein relation in order to preserve Onsager reciprocity between the phenomenological cross coefficients, the following expressions, derived from equations (2.2.21) to (2.2.24) and (2.3.7), were used to calculate the electrolyte transport constants

$$D_s = \frac{RTM_s\Lambda(z_1-z_2)\,t_1 t_2}{(z_1 z_2 F)^2}, \tag{2.6.3}$$

$$\Lambda'/\Lambda = \frac{RT}{F}\left(\frac{t_1}{z_1}+\frac{t_2}{z_2}\right), \tag{2.6.4}$$

$$D'/\Lambda = M_s\Lambda'/RT(z_2-z_1)\,\Lambda. \tag{2.6.5}$$

Here t_1, t_2 are the transport numbers of the cation and anion respectively.

The particular properties of the membrane which are required in the calculations are its thickness l, the mean pore radius a, the number of pores per unit surface area N and the surface charge constant K (or $\bar{\sigma}$ in the case of a membrane with a concentration independent surface charge density).

In the case of the Nuclepore membranes studied here the thickness was accurately measured with a transducer gauge (Mercer–Parnum type B 203 with model 500 probe) and the pore density and radii were obtainable directly by using a Zeiss Ultraphot II projection microscope.

In fact, although the surface of the Nuclepore filters is very smooth and the thickness uniform,

the manufacturer allows the pores up to 13° inclination from the normal to the surface. The pore length is therefore not quite uniform and the mean pore length a little greater than the membrane thickness l. While one might estimate a mean length of the pores correctly weighted to describe their permeability properties this refinement did not seem to be justified in view of the much greater uncertainty in the pore radius a.

An effective mean pore radius $\bar{a}$ could be determined from a simple hydrodynamic permeability experiment by making use also of the measured thickness and pore density. In the experimental section the determination of a permeability coefficient L_p defined by

$$L_p = (V_m/\Delta P)_{\Delta\psi,\,\Delta\mu_s=0} \tag{2.6.6}$$

will be described. This coefficient L_p is related to the membrane dimensions, in the range of streamline flow, by the simple expression

$$L_p = \pi\bar{a}^4 N/(8\eta l). \tag{2.6.7}$$

The values of $\bar{a}$ evaluated from l, N and L_p were always in the region of 20 % lower than a measured optically. It was invariably the case that the predicted transport properties of the membrane system agreed more nearly with those observed when the effective pore radius $\bar{a}$ was used in the calculation, in preference to a, and this procedure was adopted in the calculations reported here.

The surface charge on the membrane pores was studied by making observations on electro-osmotic flow under zero concentration and pressure difference. These measurements, which led to the value of K, are described later, in § 3.5.

The remaining system parameter required in carrying out the calculations was the thickness δ of the stagnant layers of solution in contact with the membrane; δ can be determined by a critical limiting current procedure (Scattergood & Lightfoot 1968) to be described in § 3.6.

3. Experimental

3.1. *Introduction*

The intention of the experimental programme was to demonstrate that phenomena could be observed in the well-characterized Nuclepore membranes identical to those observed by Teorell and others in sinter membranes and powder compacts and to use the data to test quantitatively the theory given above. Current–voltage curves were chosen as the primary basis for the comparison between theory and experiment and an apparatus has been designed to enable these to be determined with accuracy. Other experiments were confined to characterizing the membrane.

3.2. *The membrane apparatus*

Figures 3 and 4 illustrate the membrane cell. The membrane holder MH and the electrolyte compartments B were constructed from Perspex. They were clamped together by using longitudinal brass bolts R and S. Water-tight seals were achieved where necessary by means of rubber gaskets. The holders for the current passing electrodes CE were also constructed from Perspex. They were fitted into the sides of the compartments B by means of tapered joints. All the tubes which fitted into these compartments were of glass.

In order to facilitate repairs, all glass to Perspex joints apart from those in the membrane holder were sealed by using dental 'sticky wax'. The corresponding joints in the membrane holder were secured by using Araldite epoxy-resin.

PHILOSOPHICAL TRANSACTIONS OF THE ROYAL SOCIETY A MATHEMATICAL, PHYSICAL & ENGINEERING SCIENCES

The design of the membrane holder was selected only after exhaustive trials. It is shown in greater detail in figure 5. The membrane potential was measured by means of the silver/silver chloride electrodes A prepared by the method of Brown (1934). The electrodes were connected to the internal part of the cell by means of the salt bridges SB. These latter terminated in narrow

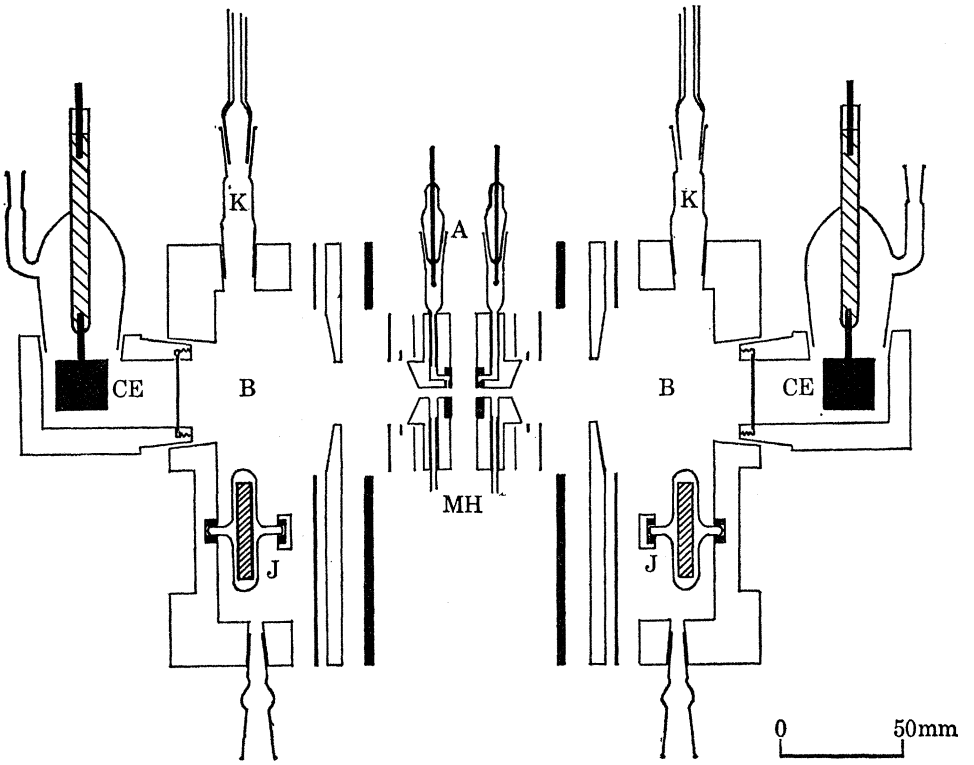

FIGURE 3. Side elevation of the membrane cell.

capillaries, 0.2 mm in diameter, set normal to the wall of the central channel C. The membrane was clamped by means of the polyethylene washers W which were sealed into the Perspex part of the holder with rubber cement.

This design of salt bridge was chosen as it did not distort the current lines in the neighbourhood of the membrane surfaces. Its general configuration corresponded with that described by Gunning & Gordon (1942). Owing to the low electrical resistances of the Nuclepore filters the distances between the salt bridge orifices and the membrane surfaces had to be kept to a minimum (approximately 1 mm between each surface and orifice).

It was found that Luggin capillaries projecting to the centre of the membrane created a serious local disturbance of the potential and current. With the arrangement adopted here it was however essential to design the membrane holder so that the current density was precisely uniform over the whole membrane surface. To ensure this condition the theory of Greenwood (1968, and private communication) was used to assess the length and diameter of the cylinders C in figure 5 such that the ratio of the radial to the axial component of the electric current density at a point in the vicinity of the cylinder wall close to the electrode orifice was less than 1×10^{-6}.

When sulphate solutions were used instead of chlorides, the silver/silver chloride probes were replaced by small calomel electrodes.

Stirring in the vicinity of the membrane surfaces was achieved by constantly flowing electrolyte through the compartments B into C, and thence to the channels U (see figure 6).

Each of the compartments B had an internal volume of 250 ml. These compartments were stirred by means of magnetically driven paddles J. Each compartment was connected to a 1 l capacity reservoir and thence, via a closed centrifugal pump P, to the appropriate channel U in the membrane holder. The electrolyte reservoirs R were of glass and the pumps were constructed from Perspex. The pump rotors were driven by external rotating magnets.

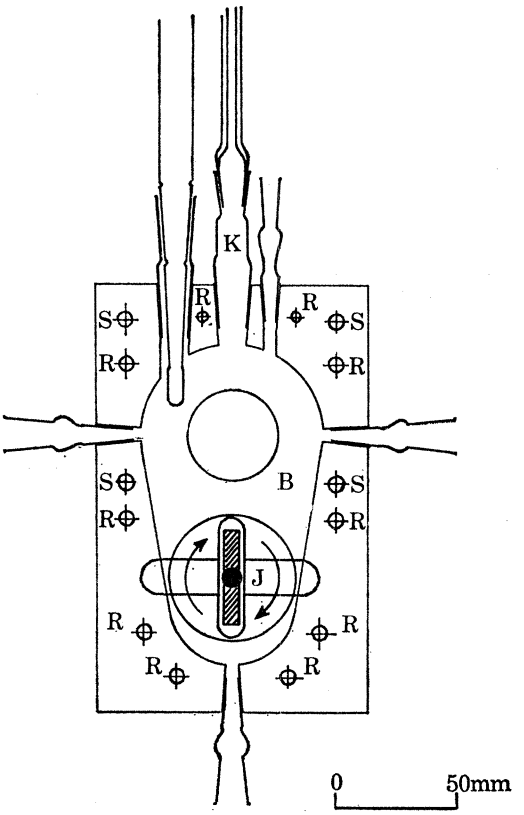

FIGURE 4. End elevation of the membrane cell.

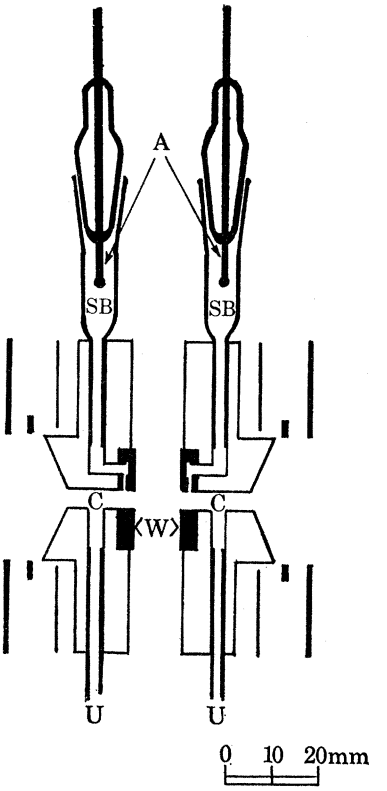

FIGURE 5. The membrane holder.

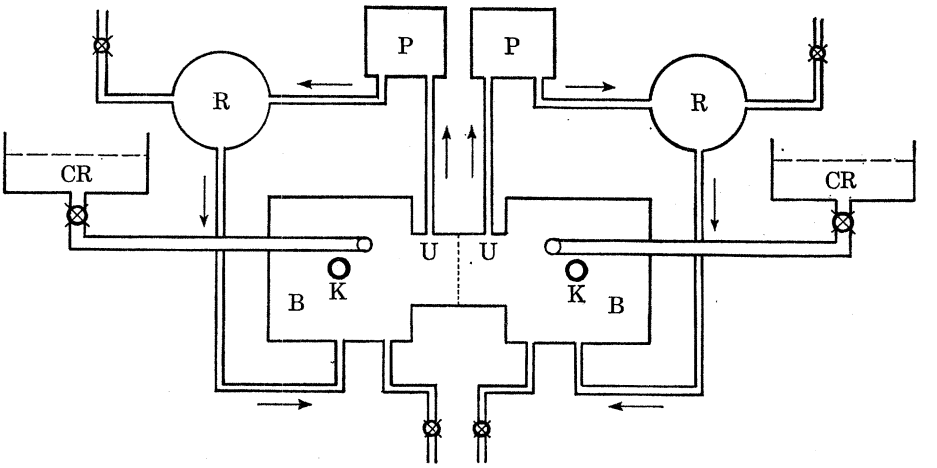

FIGURE 6. The fluid circulation circuit.

The components of each liquid circuit were connected by means of 5 mm internal diameter thick-walled PVC tubing. Each circuit was entirely closed from the atmosphere and was capable of circulating a pulse-free flow of electrolyte at the rate of 1 l/h. The general layout of these fluid circulation circuits is illustrated in figure 6.

A ground glass cone K was housed on the top of each compartment B. This facilitated connexion between the compartment and either a vertical capillary or a constant pressure reservoir.

The internal compartments of the current passing electrodes CE were separated from compartments B by ion-exchange membranes (Ionics 61 CZL-256 on the anodic side, and Ionics 111 BZL-256 on the cathodic side). The current passing electrodes were constructed from silver gauze each being plated with 1.3 mequiv of chloride.

The membrane cell and electrolyte circulating systems were housed in an air thermostat controlled to ± 0.1 K. Each electrolyte reservoir was fitted with an internal glass coil through which water from a thermostat was circulated continuously. Heat exchange with the coils controlled the electrolyte temperature in the system to within ± 0.02 K.

3.3. *The measuring and recording devices*

The potential across the electrodes A was fed to a potential divider of resistance 50 MΩ and thence, in part, to a Vibron electrometer. The electrometer output was fed either to one point of a multi-point *x*–*t* Rikadenki pen recorder, or to the *y*-terminals of an *x*–*y* recorder (Hewlett–Packard 7035 A).

A constant current was supplied to the electrodes CE from a galvanostat consisting of a high voltage a.c./d.c. converter (< 1 % ripple) connected in series with a 60 kΩ resistor. The current strength was measured either by means of calibrated moving coil ammeter or by passing the current through a standard resistance and connecting the potential across the resistance to the *x*-terminals of the *x*–*y* recorder.

Constant voltage studies were made by means of a Witton MT 1 differential potentiostat. This instrument was connected directly to the sensing electrodes A and the current electrodes CE. The potential which measured the current strength and the potential across the electrodes A were, in this case, fed direct from the potentiostat to the *x*–*y* recorder.

The pressure differential generated across the membrane during an oscillatory experiment was measured by means of a Hilger–Watt type MDC AA gas manometer. In this type of experiment vertical capillaries were mounted on to the membrane cell by means of the cones K. The diaphragm head of the manometer was connected to the top of each of these capillaries with thick-walled PVC tubing. The rise and fall of the liquid in the capillaries caused pressure changes in the closed gas space at the top of each vertical tube. The gas pressure changes were converted to a linear electrical signal by the manometer. This signal was fed to a single point of the *x*–*t* multipoint chart recorder.

The differential gas pressure ΔP_G was related to the instantaneous pressure difference ΔP_C exerted by the vertical columns of liquid on the solutions in compartments I and II of the cell by means of Boyle's law. ΔP_G can be expressed by

$$\Delta P_G = \frac{\Delta U}{U^2 - \Delta U^2}[2P_G U - U(p_I + p_{II}) - \Delta U(p_I - p_{II})], \tag{3.3.1}$$

where p_i (i = I or II) indicates the equilibrium vapour pressure in compartment i (I for the anodic and II for the cathodic compartment). Initially the liquid levels in each vertical column

were the same and a volume U of gas at pressure P_G was enclosed on each side of the manometer. Equation (3.3.1) describes the change brought about when a volume of liquid ΔU is transferred from compartment I to compartment II through the membrane. When this happens the volume of gas in tube II is decreased by ΔU and that in tube I increased by this amount.

If d_I is the density of the solution in compartment I, d_{II} the density of the solution in compartment II and d_G the density of the enclosed gas then

$$\Delta P_C = \Delta P_G + \Delta U g(d_I + d_{II} - d_G)/\pi r_t^2, \tag{3.3.2}$$

where r_t is the radius of the vertical columns and g the gravitational acceleration. By neglecting $(p_I - p_{II})$, equations (3.3.1) and (3.3.2) may be combined to yield, provided $U^2 \gg \Delta U^2$,

$$\Delta P_C = K_P \Delta P_G, \tag{3.3.3}$$

where

$$K_P = 1 + \frac{Ug(d_I + d_{II} - 2d_G)}{\pi r^2[2P_G - (p_I + p_{II})]}. \tag{3.3.4}$$

In most of our experiments capillary tubes of diameter 2 mm were used and K_P had the typical value 1.47.

Studies on the stationary states of the system were performed at fixed pressure differentials by connecting constant pressure reservoirs (CR on figure 6) to the sockets at K. Each reservoir had a surface area in excess of 0.01 m². This area was found to be sufficient to maintain a set pressure differential constant to an accuracy better than 1 %, over a period of 10 min, and under the most extreme conditions. One reservoir was kept always at a constant height and the other was supported on a jack and could be moved up or down as required. The positions of the liquid levels were registered in 10 mm diameter glass tubes connected to each reservoir. The pressure differential was read to an accuracy of ± 0.5 % by means of observing the levels in these glass tubes by using a cathetometer. It was kept constant over long periods by manual adjustment.

3.4. *Characterization of the membranes*

Nuclepore filters are made from a polymeric derivative of bisphenol-A (4,4′-dihydroxy-phenyl-2,2-propane). Each filter consists of a film penetrated by an array of nearly parallel cylindrical pores (a tolerance of up to 13° from the normal to the membrane face is permitted by the manufacturer). The pores are randomly distributed across the membrane surface having been created by etching tracks left by nuclear fission fragments. Table 1 summarizes the dimensions of the membranes and the pores determined directly as described in § 2.6.

The hydrodynamic permeability of each membrane was measured by a flow method. The permeability coefficient L_p is defined under conditions of short circuit ($\Delta\psi_m = 0$). It was not convenient to measure owing to uncertainties in sensing the membrane potential, a point that will be dealt with in more detail below. Under open circuit conditions and with $\rho_I = \rho_{II}$ equations (2.1.22), (2.2.1) and (2.2.5) show that the open circuit ($I = 0$) permeability L_p' is given by

$$L_p' = \left(\frac{V_m}{\Delta P}\right)_{I_m,\ \Delta\mu_s=0} = \frac{\pi a^4 N}{8\eta l} - \left(\frac{\sigma}{\kappa\eta}\right)^2 \frac{\pi a^2 N}{l k_s}, \tag{3.4.1}$$

where k_s is the specific conductance of the solution.

Provided the electrolyte concentration is sufficiently high the second term on the right-hand side of equation (3.4.1) may be neglected. Thus for bathing solution of 0.1 mol dm^{-3} sodium chloride and an effective surface charge of -1.0 μC cm^{-2}, $\pi a^4 N/8\eta l$ in the membranes examined

here was always greater than $(\sigma/\kappa\eta)^2\pi a^2 N/lk_s$ by a factor of 10^4. It was therefore permissible to make the approximation

$$L'_p \simeq \pi a^4 N/(8\eta l) = L_p; \tag{3.4.2}$$

L_p was measured by using the 'half-time' method. This measurement was carried out on the membrane when mounted in the membrane cell which was filled with 0.1 mol dm^{-3} solutions of sodium chloride. First a pressure differential was set up across the membrane while the vertical

Table 1. Membrane dimensions

membrane	2MA	5MB	6MC	2MD
pore diameter (optical)/μm	0.52	0.76	1.02	2.02
standard deviation pore diameter/μm	0.05	0.09	0.13	0.19
number of pores/10^9 m^{-2}	270	100	50.7	22.9
standard deviation/10^9 m^{-2}	41	10	2.5	3.2
percentage of pore overlap (manufacturers data)	0.42	0.56	0.93	3.26
membrane thickness/μm	12.0	11.2	12.4	9.15

Table 2. Permeability coefficients

	$10^8 L_P$/m Pa^{-1} s^{-1}	
membrane	from flow measurements	from data in table 1
2MA	2.35	3.82
5MB	3.19	8.90
6MC	5.62	9.85
2MD	36.2	85.2

capillary tubes were in place. The cell was then isolated and the subsequent fall in pressure differential followed as a function of time by observing the liquid levels in the capillary tubes. The time $t_{0.5}$ taken for the differential height in the vertical capillaries to fall to half its original value was then recorded. The permeability coefficient was calculated from this by using the relation

$$L_p = \frac{\ln 2}{2d_s g t_{0.5}} \left(\frac{r_t}{j}\right)^2, \tag{3.4.3}$$

where r_t is the radius of the vertical capillary, j the radius of the exposed disk of membrane, d_s the density of the solution in the cell.

Although this observation was always made on previously unused membranes, the observed permeability coefficient L_p was always considerably smaller than the value of L_p calculated from the membrane structure data in table 1 by means of equation (3.4.2) (see table 2). After exhaustive trials it was concluded that the pore radii effective for solution flow were less than the optically measured radii. No conclusive evidence was forthcoming as to the exact reason for this.

3.5. *Membrane electrical properties*

It proved to be impossible to measure accurately the electrical resistance R_m of the membrane owing to uncertainty in the resistance R_s of the solution between the salt bridges and the membrane. R_s was always an order of magnitude higher than R_m. The observed total resistances were obtained from the slopes of plots of voltage against current with the membrane in its holder assembled in the cell.

It was hoped that R_m might be obtained by making successively measurements of the resistance

with and without the membrane in its holder while both sides of the cell were filled with the same concentration of electrolyte. In practice it was not possible to dismantle and reassemble the membrane holder in an exactly repeatable manner. Variations of up to $\pm 15\,\%$ occurred in R_s whenever the holder was dismantled and reassembled. These variations arose as the gaskets W distorted slightly when the membrane holder was tensioned. Although these variations prevented the absolute measurement of R_m, the observed resistances were consistent and remained constant to within the instrumental errors of $\pm 2.5\,\%$ so long as the holder remained assembled.

The effective surface charge associated with the walls of the membrane pores was determined by measuring electro-osmosis. The electro-osmotic cell was based on that used by Mackay & Meares (1959) and by McHardy, Meares, Sutton & Thain (1969) except that the electrodes were inserted directly into the main compartments of the cell and the membrane holder was modified so that it could clamp a Nuclepore filter. The electro-osmotic cell was mounted in an air thermostat kept constant to ± 0.1 K. The current was supplied by a high tension battery and the current strength was measured by passing it through a standard resistance in series with the cell and across which the potential difference was recorded. As the Nuclepore filters are highly permeable it was found especially important to ensure that the capillaries used for measuring the electro-osmotic flow were always perfectly horizontal.

In each experiment a solution of the desired concentration was flowed into both sides of the cell and all trapped air bubbles removed. After allowing time for thermal equilibration the electro-osmotic flow was measured at five current strengths. The volume flow rate was obtained by timing the passage of a meniscus between consecutive points on an etched glass scale clamped behind the capillaries. Twelve sets of volume flow measurements, six in each direction were made at each current strength.

The surface charge density σ at each concentration was obtained by averaging the values obtained from the equation

$$\sigma = -\eta\kappa k_s (V_m/I_m)_{\Delta P,\,\Delta\mu_s=0}. \tag{3.5.1}$$

This equation may be obtained from equations (2.1.22), (2.2.1) and (2.2.5). If I_0 is the current passed through the membrane, t the time taken by the meniscus to traverse a distance h in the capillary, and r_t the radius of the capillary, equation (3.5.1) may be expressed as

$$\sigma = -\pi r_t^2 \eta\kappa k_s (h/I_0 t). \tag{3.5.2}$$

Plots of I_0 against h/t gave good straight lines. A typical plot is shown in figure 7. Some typical values of σ are given in table 3.

It can be seen that σ decreased with decreasing concentration for all membranes and in every electrolyte. The membrane matrix polymer is not intrinsically ionizable and consequently it is natural to suspect that its surface charge in electrolyte solutions might be due to the adsorption of anions. The empirical generality of the Freundlich isotherm prompts one to plot $\lg\sigma$ against $\lg\rho_s$. This was found to give a series of almost parallel straight lines.

The lines could be represented, within the experimental uncertainty, by the single equation

$$\sigma = K\rho_s^{\frac{1}{3}}, \tag{3.5.3}$$

where K is an empirical constant. Such a cube root dependence of σ on the concentration in very dilute solutions has been predicted by Benton & Elton (1958). The value of K required to fit equation (3.5.3) to equation (3.5.2) at each concentration is listed in table 3 along with σ. K was found to be a constant to within $\pm 16\,\%$ for each membrane and electrolyte over the range

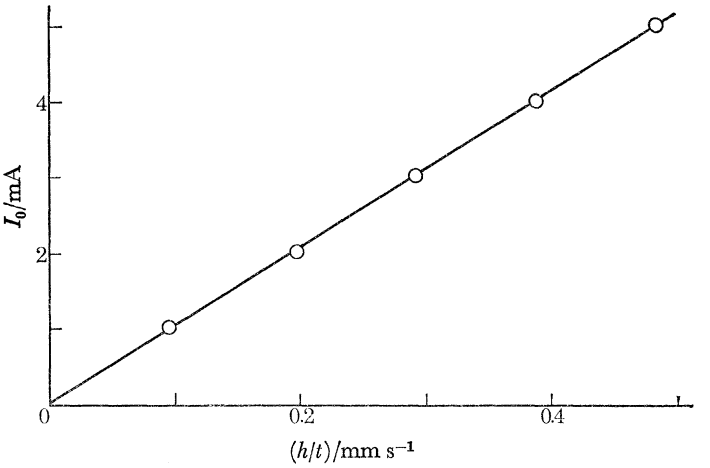

FIGURE 7. I_0 against h/t for membrane 1 MA in 0.0135 mol dm^{-3} NaCl. $\partial(h/t)/\partial I_0 = 98$ mm s^{-1} A^{-1}.

TABLE 3. TYPICAL VALUES OF SURFACE CHARGE DENSITIES AND CONSTANTS K

(*a*) *Different membranes in* NaCl *solutions*

membrane	concentration / mol dm^{-3}	surface charge density, σ / mC m^{-2}	surface charge constant, K / mC m^{-1} kg$^{\frac{1}{3}}$
1 MA	0.103	−8.08	−4.44
	0.101	−8.41	−4.65
	0.0515	−6.45	−4.47
	0.0135	−3.94	−4.26
	0.00500	−3.47	−5.23
5 MC	0.100	−5.16	−2.86
	0.100	−5.50	−3.05
	0.0530	−3.79	−2.60
	0.0511	−3.50	−2.43
	0.0106	−3.38	−2.61
	0.00540	−1.69	−2.48
	0.00128	−1.35	−3.20
1 MD	0.0990	−6.43	−3.58
	0.0509	−5.00	−3.47
	0.0156	−3.45	−3.56
	0.0112	−3.36	−3.87
	0.00507	−2.98	−4.47

(*b*) *Different electrolytes in membrane* 5 MC

electrolyte	concentration / mol dm^{-3}	surface charge density, σ / mC m^{-2}	surface charge constant, K / mC m^{-1} kg$^{\frac{1}{3}}$
NaCl	see part (*a*)		
$MgCl_2$	0.0502	−2.27	−1.35
	0.0102	−1.49	−1.50
	0.00520	−1.58	−2.00
	0.00109	−0.880	−1.87
Na_2SO_4	0.0511	−7.58	−3.91
	0.0106	−5.32	−4.64
	0.00526	−4.18	−4.60
	0.00109	−2.44	−4.54
HCl	0.0104	−3.22	−4.45
	0.00529	−2.38	−4.12
	0.00106	−1.07	−3.12

of ρ_s studied. It varied from membrane to membrane but was $-4.5 \pm 1.0 \times 10^{-3}\,\mathrm{cm^{-1}\,kg^{-\frac{1}{3}}}$ in NaCl.

3.6. *Thickness of stagnant solution layers*

Despite the provision of mechanical paddle stirrers in the cell body and the maintenance of a steady flow in the membrane holder by the solution circulating system, it was not desirable to agitate the solution in contact with the membranes faces very violently. As a result the interfacial concentrations differed from the bulk solution concentrations. The effect of this on the membrane fluxes is included in the theory by the parameter δ.

TABLE 4. THICKNESS OF STAGNANT LAYERS

control settings	film thickness (side I)	film thickness (side II)
V	μm	μm
208	144	126
212	110	106
220	104	101

The method of Scattergood & Lightfoot (1968) was used to determine the effective thickness δ of the stagnant layers adjacent to the membrane. A sheet of silver foil 0.13 mm thick, with a wire lead attached to its edge, was clamped into the membrane holder in place of the membrane. The ion-exchange membranes were removed from the electrode holders CE, and the normal current passing electrodes were replaced by silver anodes of large area. The cell was filled with a solution $5 \times 10^{-3}\,\mathrm{mol\,dm^{-3}}$ with respect to silver nitrate, and $1\,\mathrm{mol\,dm^{-3}}$ with respect to sodium nitrate.

The current–voltage characteristics of each half cell were determined separately and under different conditions of mechanical stirring and circulation pumping. In each experiment the silver foil was made the cathode. A high-quality potential divider was used to control the current supply to the electrodes from a 2.5 V accumulator. The current was measured by passing it through a standard resistor in series with the half cell and recording the potential difference across the resistor using the *x*–*y* plotter. The potential between the silver foil and each anode was detected with the Vibron electrometer and displayed on the *x*–*y* recorder. The current–voltage plots showed well-defined plateaux which corresponded with the limiting currents I_∞.

The thickness of the polarized layers δ under these experimental conditions may be estimated by using the relation

$$\delta = D_{\mathrm{Ag}} F c_{\mathrm{Ag}} / I_\infty, \tag{3.6.1}$$

where D_{Ag} is the diffusion coefficient and c_{Ag} the molar concentration of Ag^+ ions.

The values of δ are summarized in table 4. They were repeatable to within $\pm 7.5\,\%$. The control voltage setting shown in the table is related to the speed of mechanical stirring and the rate of circulation of solution. A setting of 212 was used in all the oscillation and steady flux experiments.

3.7. *Measurement of current–voltage curves*

Although the experiments were carried out under a wide variety of conditions, they were all performed by using the same procedure. The following description of a single experiment will therefore serve as a typical example for the whole.

Aqueous solutions of NaCl at $0.1\,\mathrm{mol\,dm^{-3}}$ and $0.01\,\mathrm{mol\,dm^{-3}}$ were prepared volumetrically from the dried Analar grade salt and distilled deionized water. Each solution was then filtered through a 0.05 μm Millipore filter. (The filter was preconditioned so as to remove most of the

PHILOSOPHICAL TRANSACTIONS OF THE ROYAL SOCIETY A MATHEMATICAL, PHYSICAL & ENGINEERING SCIENCES

wetting agent contained within it.) Both solutions were degassed by maintaining them at 60° for at least 10 min under a water pump vacuum.

A Nuclepore filter of 1.0 μm nominal pore diameter was placed in a membrane holder in which 12 mm² membrane were exposed. The filter and holder were inserted into the cell and both electrolytes transferred into the cell and into the ancillary fluid circulation circuits. The dilute

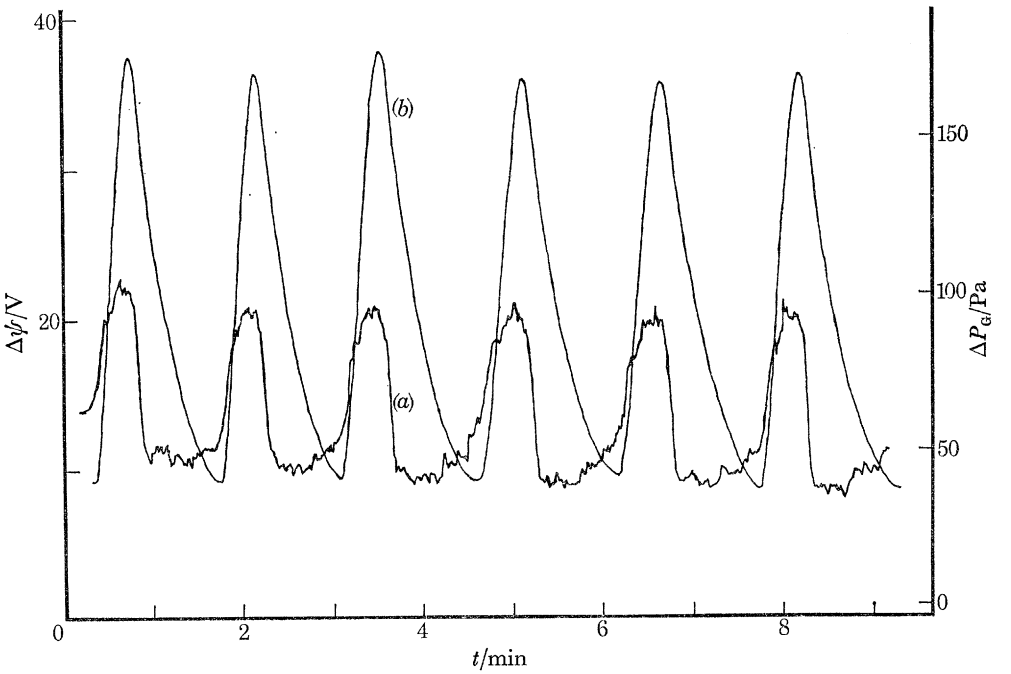

FIGURE 8. Undamped oscillations across a membrane with 2 μm pores. Variations in the potential $\Delta\psi$ between electrodes A are recorded by trace (*a*), and variations in the pressure differential ΔP_G are recorded by trace (*b*). The traces are plotted as a function of the time *t*. The membrane separated solutions of 0.1 and 0.01 mol dm^{-3} NaCl, and the cell was fitted with 3 mm diameter vertical capillaries. A current density of 1.8×10^3 A m^{-2} was used.

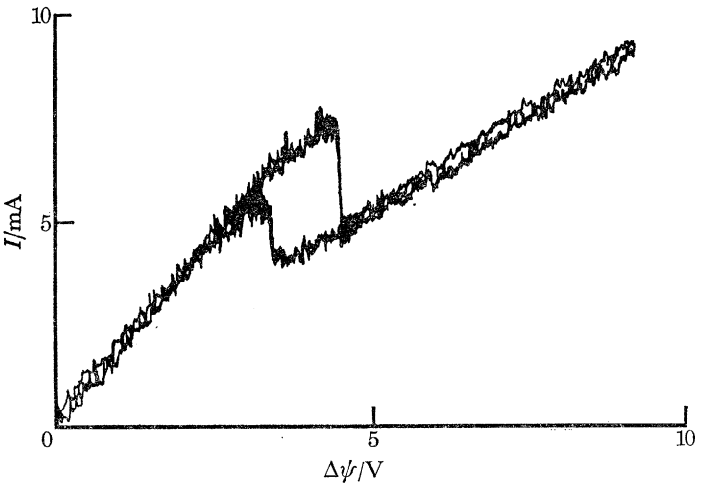

FIGURE 9. Potentiostatic current plotted against voltage. The trace was obtained using a pressure clamp of −687 Pa across 13 mm² of a membrane with 0.5 μm pores. The membrane separated solutions of 0.1 and 0.01 mol dm^{-3} NaCl.

solution filled the anodic and the concentrated solution the cathodic half of the apparatus. Both current-passing electrode compartments were filled with 0.1 mol dm^{-3} aqueous NaCl.

After removing trapped air bubbles and allowing the solutions to equilibrate thermally a run was carried out to check that the membrane was capable of producing sustained oscillations. During this and all subsequent runs the electrolytes were always kept vigorously stirred.

Capillary tubes of 3 mm bore were inserted into the sockets at K, and the electrolyte levels were then raised to the vertical midpoints of these tubes. The manometer was connected to the tubes and a constant current was passed between the electrodes CE. Provided the current density was

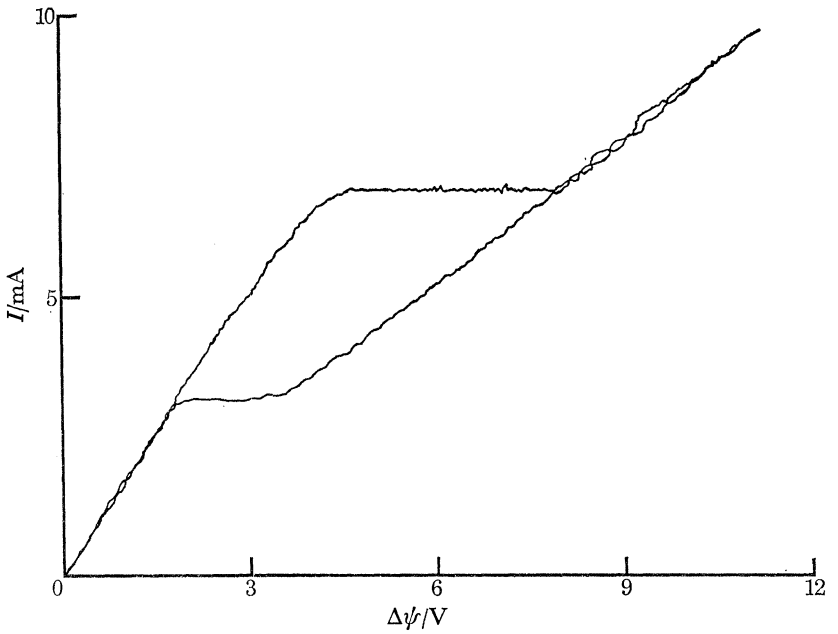

FIGURE 10. Galvanostatic current plotted against voltage. The trace was obtained by using a pressure clamp of −589 Pa across 13 mm^2 of a membrane with 0.5 μm pores. The membrane separated solutions of 0.1 and 0.01 mol dm^{-3} NaCl.

sufficiently high, in the case under discussion 1 mA mm^{-2}, oscillations of the pressure differential and membrane potential were observed. Figure 8 illustrates a typical trace obtained from this type of experiment. The electro-osmosis always occurred in the direction of the cation current.

After observing the periodicity of the system the stationary states were examined. This required the vertical capillaries to be replaced by the constant level reservoirs in the sockets of K. Plots of current against membrane potential were then obtained at a series of constant pressure differentials ΔP, taken in the sequence of increasing ΔP. These records were obtained by first employing the potentiostat, and then were repeated by using the galvanostatic circuit. In the majority of cases galvanostatic records only were taken. Owing to the resistance of the solution layers between the probe electrodes and the membrane surfaces, the potentiostatic control system did not maintain the true membrane potential constant. The results could not therefore be interpreted as readily as those measured under galvanostatic conditions.

The x–y plotter was used for recording all current versus membrane potential plots. In every experiment the current or potential, whichever was appropriate, was controlled by hand. Each current or voltage range was scanned by slowly increasing and then by decreasing the electrical supply. Especial care was taken in the nonlinear regions close to the points of flip-over, so tha

true stationary states were recorded. Each complete current versus membrane potential plot was repeated at least once at each pressure differential. Figures 9 and 10 illustrate the characteristic flip-flop curves that were obtained by these methods. Four different pressure differentials were examined in each stationary state run.

The value of the hydrodynamic permeability coefficient L_p of the membrane and the compositions of the electrolyte solutions were monitored at regular intervals throughout the experiment. The electrolyte solutions were monitored by withdrawing 50 ml aliquots from each side of the cell. The pH of each of these samples was measured by means of a Radiometer pH meter and their conductivities were recorded with a thermostatted conductivity cell and a Wayne–Kerr Universal Bridge.

4. Results

4.1. *General considerations*

A series of experiments was carried out using four grades of Nuclepore filters with nominal pore diameters 0.5, 0.8, 1.0 and 2.0 μm. The effects of varying both the type and concentration of the electrolyte solutions on the membranes with 1.0 μm pores were also examined. Table 5 lists the principal experiments conducted during this investigation.

Table 5. Summary of principal experiments performed together with membrane and apparatus characteristics

run	nominal pore size† / μm	concentration / mol dm^{-3}	electrolyte	$10^8 L_p$ / m Pa^{-1} s^{-1}	K / mC m^{-1} kg$^{-\frac{1}{3}}$	l / μm	10^{-10}N / pore m^{-2}	type of measurement‡
1MA	0.5	0.1/0.01	NaCl	2.28	−4.45	12.0	27	O, G
2MA	0.5	0.1/0.01	NaCl	2.35	−9.84	12.0	27	O, G, P
5MB	0.8	0.1/0.01	NaCl	3.19	−7.70	11.2	9.0	O, G
6MC2	1.0	0.1/0.005	NaCl	5.62	−5.21	12.4	5.0	O, G
6MC3	1.0	0.1/0.01	NaCl	5.62	−5.21	12.4	5.0	O, G
6MC4	1.0	0.05/0.005	NaCl	5.62	−5.21	12.4	5.0	O, G
6MC5	1.0	0.05/0.005	NaCl	5.62	−5.21	12.4	5.0	O, G
6MC6	1.0	0.05/0.005	$MgCl_2$	5.62	−5.23	12.4	5.0	O, G
6MC7	1.0	0.05/0.005	Na_2SO_4	5.62	−9.70	12.4	5.0	O, G
1MD	2.0	0.1/0.01	NaCl	30.8	−3.67	9.15	2.3	O, G
2MD	2.0	0.1/0.01	NaCl	36.2	−4.35	9.15	2.3	O, G

† Manufacturer's specifications.

‡ Type of measurement: O = oscillations, G = galvanostatic stationary states, P = potentiostatic stationary states.

For all membranes $\delta = 106$ μm.

Observations were made first on the periodicity of the system with vertical capillaries in place and then on the steady states. The period and amplitude of the oscillations tended to increase somewhat with time during a run. Many tests showed that this effect was caused principally by dirt silting up the membrane pores and hence decreasing the value of L_p. Despite extensive efforts this silting effect could not be entirely eradicated.

In order to minimize drifts in the hydrodynamic permeability only one set of oscillation and one set of steady-state measurements was made on each exposed area of membrane. Each steady current–voltage plot in a set was determined twice. The data in all the tables of results give the average values of the two determinations.

4.2. *Oscillatory behaviour*

Undamped oscillations were only obtained if a number of important conditions were fulfilled. The maximum exposed area of membrane capable of producing undamped oscillations was found to be 38.5 mm². The best results were obtained with either 12.6 or 7.1 mm² of membrane exposed. No limitation was found on the cross-section of the vertical capillary columns. Capillaries of diameters ranging from 0.5 to 10 mm were used successfully. The oscillations were unaffected by changes in stirring provided the speed of the stirrers J was greater than 100 rev/min and the fluid circulation rate exceeded 500 ml/h. The oscillations became either damped or irregular if the stirring fell below these strengths.

The absolute concentrations of the electrolytes and their ratio were important for the production of regular periodicity. Oscillations disappeared if the concentration ratio fell far below 10 : 1. It was necessary for the absolute concentrations of the electrolytes to be neither too high nor too low. Oscillations were obtained with NaCl solutions between 0.1 and 0.005 mol dm^{-3}, but no oscillations were obtained with either solution at 0.5 or 0.001 mol dm^{-3}. Undamped oscillations were also observed when using solutions of Na_2SO_4 and $MgCl_2$ at concentrations of 0.05 and 0.005 mol dm^{-3}.

A critical current density existed for each experimental configuration below which oscillations either disappeared or became damped. Above this critical current density oscillations could be maintained up to the point at which the current induced pH changes in the electrolyte.

It was found that deliberately lowering pH decreased the amplitude of the oscillations in pressure, whereas increasing the pH had the opposite effect. In both cases the period of oscillation was considerably increased. With large pH changes the periodic behaviour of the system completely disappeared.

Oscillations were observed with periods ranging from 0.2 to 20 min according to the type of membrane, the cell configuration, and the types and concentrations of the electrolytes. A very small increase in period occurred with increasing current density.

Comparison of our results with those of Teorell (1959*a*) and Drouin (1969) has demonstrated that there are many features in common between the polycarbonate Nuclepore and the glass sinter membrane systems. Our experimental arrangement for producing periodicity differed slightly from that used by the earlier workers because we enclosed the gas above the liquid in the vertical capillary tubes and connected it to the manometer. This alteration was not of great importance because the volume flux was still linearly related to the rate of change of pressure differential across the membrane. Furthermore, tests showed that oscillations could readily be obtained when using open capillaries just as employed by Teorell.

The system described here not only produced oscillations and flip-flop behaviour of the same form as were observed by Teorell and Drouin, but the phenomena depended on the same experimental parameters such as the concentration ratio of the electrolytes, the cell geometry and the current density.

It was concluded that Nuclepore membranes besides being accurately characterizable, were capable of producing the same phenomena as have been observed in composite glass membranes.

4.3. *Steady-state behaviour*

Typically, the membrane may exist in either one of two stable states. These are a low resistance state when the pores are filled mainly with concentrated solution and a high resistance state when

they are filled mainly with the dilute solution. Transitions between these states may be induced by altering the magnitude of either the electrical current or the hydrostatic pressure differential. Each stable state may be characterized by the electrical resistance of the membrane. Transitions between the stable states can be characterized by the value of the electric currents at the 'flip' (upper) and 'flop' (lower) points under a given hydrostatic pressure differential. These characteristic parameters are indicated on the current–voltage diagram shown in figure 11.

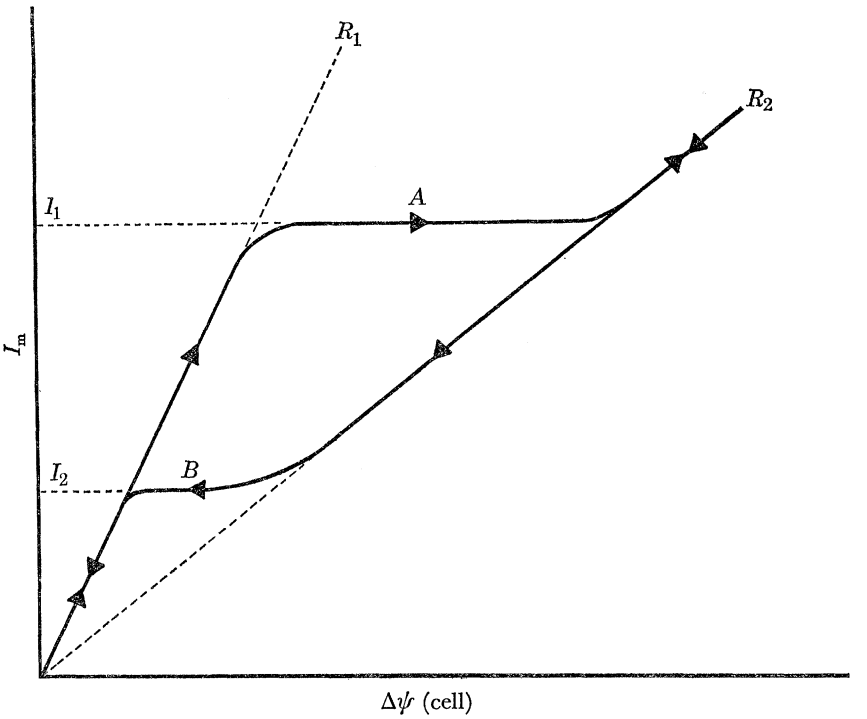

FIGURE 11. Generalized flip-flop of current I_m against cell potential $\Delta\psi$ (cell). Flip-over is marked A, flop-over is marked B, R_1 and R_2 are the limiting resistances, and I_1 and I_2 the flip and flop currents respectively.

In every situation where undamped oscillations were observed it was possible also to obtain flip-flop behaviour in the stationary states. The membrane potentials at the points of flip and flop increased in magnitude with increasing value of the clamped pressure differential. The stationary states of the system were found to be much more repeatable than the oscillations. Results obtained when using the galvanostat agreed well with those produced by using the potentiostat.

The limiting resistances observed in the membrane cell, R_1 and R_2, were obtained by drawing tangents to the virtually straight portions of the current–voltage plots at the lowest and highest current densities studies. These observed resistances, estimated from the current and potential difference between the probe electrodes in the membrane cell, may be thought of as the sum of five contributions. These are: the membrane resistance, the resistances of the two stagnant solution layers at the membrane/solution interfaces and the resistances of the two layers of bulk solution between the hypothetical outer boundaries of the stagnant layers and the probe electrodes. The distances of the probes from the membrane were much greater than the thickness δ of the stagnant layers. Each time the membrane holder was reassembled with a fresh membrane the latter lay slightly differently with respect to the probes. This had a big effect on the total resistance between the probes because the specific resistance of the bulk solution on one

TABLE 6. STATIONARY STATE FLIP-FLOP DATA

Membranes of different pore size in 0.1 – 0.01 mol dm^{-3} NaCl solutions

	observed			predicted			
run	I_1 / A m^{-2}	I_2 / A m^{-2}	ΔR / $10^{-4}\,\Omega\,m^2$	I_1 / A m^{-2}	I_2 / A m^{-2}	ΔR / $10^{-4}\,\Omega\,m^2$	$-\Delta P$ / Pa
2MA	253	–	65	162	156	31	196
	321	199	52	198	173	31	294†
	366	206	67	243	190	31	392
	439	264	53	295	207	30	491
	570	260	68	353	222	30	589
	620	312	55	418	237	30	687†
	801	351	63	493	256	30	785
5MB	795	557	34	218	181	40	196
	975	612	45	536	261	39	491
	1140	694	41	824	315	38	687
	1330	837	36	1320	392	37	981
6MC3	439	–	38	309	282	37	98.1
	627	356	43	554	361	37	196
	771	414	46	886	434	37	294
	900	480	44	1280	503	37	392
	1090	586	46	1710	570	37	491
	1440	867	37	2660	698	37	687
2MD	1060	418	32	1080	555	29	49.1
	2130	686	30	1740	670	28	73.6
	2760	753	14	2520	784	28	98.1

† Potentiostatic (otherwise galvanostatic).

TABLE 7. STATIONARY STATE FLIP-FLOP DATA

Effect of concentrations and type of electrolyte on one membrane.

	observed			predicted			
run	I_1 / A m^{-2}	I_2 / A m^{-2}	ΔR / $10^{-4}\,\Omega\,m^2$	I_1 / A m^{-2}	I_2 / A m^{-2}	ΔR / $10^{-4}\,\Omega\,m^2$	$-\Delta P$ / Pa
6MC2	517	223	113	219	133	86	78.5
	699	286	101	446	165	85	177
	1360	584	94	1230	230	84	392
6MC3	see table 2						
6MC4	326	147	116	257	179	65	196
	519	238	120	587	250	65	392
	837	321	107	992	316	65	589
6MC5	322	167	108				196
	610	236	112	as for 6MC4			392
	900	393	107				589
6MC6	502	–	35	220	211	47	49.1
	774	248	63	334	256	46	98.1
	1100	264	56	488	297	46	147
	1720	887	37	686	353	44	196
6MC7	315	218	92	360	181	41	196
	469	293	70	884	263	41	392
	619	335	73	1500	341	41	589
	877	368	57	2160	415	41	785
	1000	393	42	2830	488	41	981

side was normally about ten times that on the other. Thus the observed total resistance differed from that across the membrane and stagnant layers by an unknown amount which, although it remained constant in any set of experiments with one membrane specimen, varied whenever a new membrane was fitted. The quantity it was meaningful to compare between theory and experiment was therefore the change in resistance $(R_2 - R_1)$ between the high and low resistance states. This resistance change, listed as ΔR, is given in the tables of results.

Tables 6 and 7 give observed values of the flip and flop currents I_1 and I_2 and the resistance changes ΔR in some of the more important series of experiments. Repeated readings taken in any one run agreed to within $\pm 3\,\%$. A comparison of run 6MC4 with run 6MC5 indicates the degree of repeatability between separate experiments. It can be seen that the correlation between these two runs, each carried out on a different piece of the same membrane, was better than $\pm 10\,\%$.

5. Discussion

5.1. *Nonlinearity*

The characteristic behaviour of this system arises from a complex interplay between the electro-osmotic and hydrodynamic permeabilities of the membrane. This interplay is expressed in equations (2.3.15) and (2.3.25). These may be combined to give

$$\bar{\nu} l = \frac{a^2}{8\eta}(\Delta P - \Delta P_0) + \frac{K D_s}{\beta \eta}\left\{\frac{6[(1/\rho_I^m)^{\frac{1}{6}} - (1/\rho_{II}^m)^{\frac{1}{6}}] + \Gamma}{\bar{\nu} l + D_s \ln(\rho_I^m/\rho_{II}^m)}\right\}(\Delta\psi - \Delta\psi_d). \tag{5.1.1}$$

Numerical solutions of equation (5.1.1) have been evaluated, by the procedures of § 2.5, for the values of the membrane and solution parameters characteristic of some of the experiments listed in table 5. A sample of these numerical solutions is plotted in figure 12 for part of the range covered in run 6MC3. It may be seen in figure 12*a* the relation between the volume flux and the membrane potential diverges progressively further from linearity as the pressure differential is increased. In physical terms, the nonlinearity of equation (5.1.1) is due to the dependence of the electro-osmotic permeability upon the space charge in the double layer at the pore walls and hence upon the concentration of the electrolyte.

Equation (2.3.28) relates the current density to the membrane potential. It expresses the fact that the electrical resistance of the membrane depends upon the concentration profile of the electrolyte within it. This profile is greatly influenced by the direction and magnitude of the volume flux. In figure 12*b* the characteristic S-shape of the resistance–potential plot is shown.

Figure 12*c* shows that the plot of current versus membrane potential is predicted to have an N-shape, sometimes called a dynatron characteristic.

When there is a large pressure differential across the membrane the theory predicts multi-valued solutions over a range of membrane potentials and Kobatake & Fujita (1964) have discussed the theoretical implications of these. In the present work the pressures were too small for such solutions to be expected except in run 6MC7 at $\Delta P = -785$ and -981 Pa.

The flip-flop phenomena observed under apparently potentiostatic conditions in our membrane cell (see, for example, figure 9) were not due to multi-valued solutions of the membrane flux equation. They arose because there were thick liquid layers separating the membrane surfaces and the probe electrodes. These liquid layers added two resistances in series with the membrane. As the potentiostatic condition could only be fulfilled between the electrode probes, true potentiostatic conditions across the membrane faces were not obtainable.

The effect was accentuated because the resistances of the liquid layers were larger than the membrane resistance. The major part of the potential drop between the probes occurred across these liquid layers and this caused the hysteresis loops in our potentiostatic studies of the current–voltage relation.

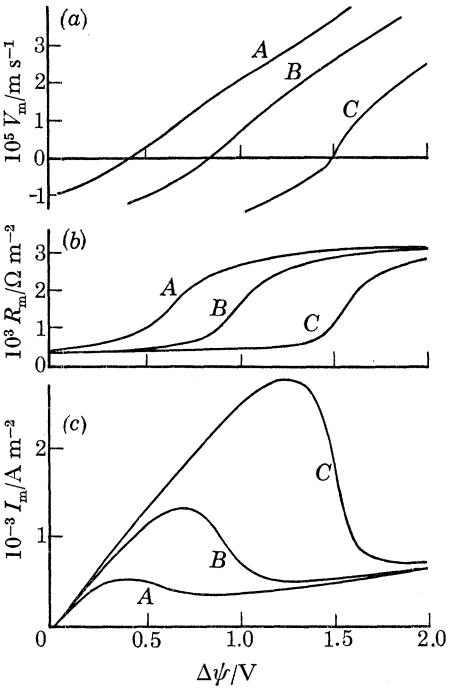

FIGURE 12. Predicted results of run 6MC3. Curve A, $\Delta P = -196$ Pa; curve B, $\Delta P = -392$ Pa; curve C, $\Delta P = -687$ Pa. (a) Volume flow V_m, (b) membrane resistance R_m, (c) electrical current I_m, each expressed as a function of membrane potential $\Delta\psi$.

5.2. *Observed and calculated current–voltage curves*

The main purpose of the calculations performed as described in § 2.5 has been to construct theoretical versions of the current–voltage curves which could be recorded directly in the membrane cell. That is to say, where the potential difference is the sum of the potential differences across the membrane, the stagnant films and the well-stirred layers of solution between the potential probes and the stagnant films.

The theoretical values of the flip-over and flop-over currents I_1 and I_2 were taken as the values of I_m at the maximum and minimum respectively in the predicted curves. The theoretical resistances R_1 and R_2 were given by the slopes of the current–voltage curves far below and far above the flip-flop region. The theoretical values are listed in the tables of results alongside the observed values.

When comparison is made between the observed and predicted characteristic parameters of the current–voltage curves it should be borne in mind that the theoretical calculations are based exclusively on clearly defined and measureable properties of the membrane, solutions and apparatus. There are no adjustable parameters. Furthermore, a number of assumptions were made, for example that all solutions were ideal, in order to obtain the final equations in a form sufficiently tractable for calculation procedures to be clearly specified. In these circumstances it is not appropriate to expect an exact correspondence between observed and predicted currents

and resistances. It is more important to test whether the theory correctly predicts the trends in behaviour which are found on varying the controllable parameters of the membrane system.

Two general observations may be made. The predicted values of ΔR frequently agree, within the experimental significance, with the observed values but in some cases the predicted ones tend to be a little too low. The predicted flip-over and flop-over currents I_1 and I_2 tend to be too small in the membranes with the finest pores and in reasonable agreement with experiment for larger pores. The agreement with theory of the lower transition current I_2 is considerably better than that of the upper one I_1.

Factors that either decrease the hydrodynamic permeability or increase the electro-osmotic permeability of the membrane are expected to make the system less sensitive to changes in pressure. That is to say, at a given ΔP both I_1 and I_2 should be smaller and they should increase less for a given increase in ΔP. These tendencies may be clearly seen when the data are examined in detail but they are not immediately obvious because the controlling factors L_p and K could not be varied independently and at will.

5.3. *Effect of membrane properties*

Attention should be turned first to the results of runs 2 MA, 5 MB, 6 MC 3 and 2 MD shown in tables 5 and 6. The electrolyte concentrations were kept constant in these experiments but

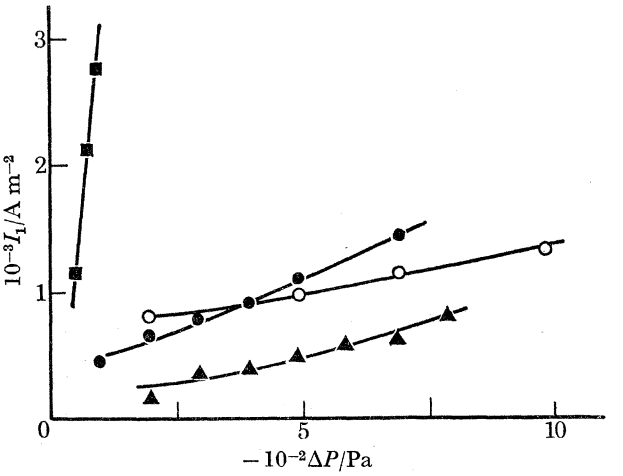

FIGURE 13. Observed flip currents I_1 plotted against applied pressure differential ΔP for run 2 MA ▲, run 5 MB ○, run 6 MC 3 ●, and run 2 MD ■.

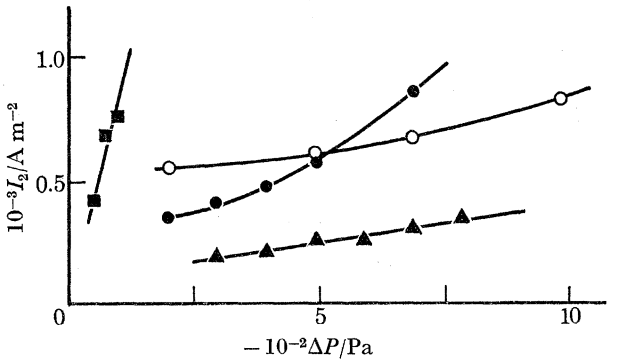

FIGURE 14. Observed flop currents I_2 plotted against applied pressure differential ΔP for run 2 MA ▲, run 5 MB ○, run 6 MC 3 ●, and run 2 MD ■.

L_p increased and K decreased in the order of the runs listed above. The changes in L_p and K should both produce the same trends in the currents I_1 and I_2, and in their sensitivity to changes in the pressure differential. It is shown in figures 13 and 14 that these predictions were borne out by experiment. The only serious discrepancy between theory and observation arose in run 5 MB where the observed values of I_1 and I_2 were higher than predicted especially at low values of ΔP. No satisfactory reason has been found for this. The results show clearly that decreasing L_p and, at the same time, increasing K decreases I_1 and I_2. It also decreases the slopes of the curves of I against ΔP.

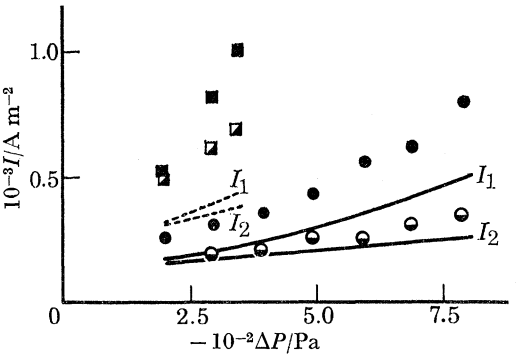

FIGURE 15. Flip and flop currents I_1 and I_2 plotted against applied pressure differential ΔP for runs 1 MA and 2 MA. Observed flip currents I_1 indicated by ■ for run 1 MA and ● for run 2 MA, and observed flop currents I_2 indicated by ◪ for run 1 MA and ◒ for run 2 MA. Predicted values of flip and flop currents shown as broken curves for run 1 MA and as solid curves for run 2 MA.

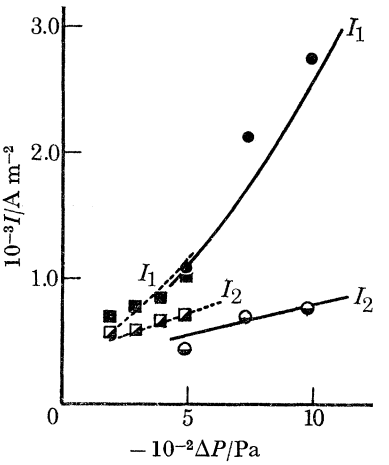

FIGURE 16. Flip and flop currents I_1 and I_2 plotted against applied pressure differential ΔP for runs 1 MD and 2 MD. Observed flip currents I_1 indicated by ■ for run 1 MD and ● for run 2 MD, and observed flop currents I_2 indicated by ◪ for run 1 MD and ◒ for run 2 MD. Predicted values of flip and flop currents shown as broken curves for run 1 MD and as solid curves for run 2 MD.

It may be noted that in runs 6 MC 3 and 2 MD that K differed by only about 20 % while L_p in 2 MD was the larger by more than sixfold. The effects of varying L_p and K independently can be seen more clearly however in figure 15. This figure shows I_1 and I_2 against ΔP for two membranes. In 1 MA and 2 MD K was almost constant but L_p was sixteen times larger in the latter membrane. Clearly I_1 and I_2 and their slopes are much greater in the membrane with the wider pores. On the other hand, L_p was almost the same in 1 MA and 2 MA but K was more than

twice as large in 2 MA. The graph shows that in 2 MA, the membrane with the larger electro-osmotic permeability, I_1 and I_2 and the slopes were less than half as large as those in 1 MA.

It was found that different samples of nominally similar membranes had somewhat different values of L_p and K. Figure 16 compares the predicted and the observed results of runs 1 MD and 2 MD. Table 5 shows that the values of L_p and K were both higher in run 2 MD than in 1 MD. The increased L_p should increase the values of I_1, I_2 and the pressure sensitivity of 2 MD compared with 1 MD, whilst the difference in K should have the opposite effect. The theory predicted that the most significant difference between these runs should be a higher set of I_2 for 1 MD relative to 2 MD. Figure 16 shows this prediction to have been exactly fulfilled. The quantitative correspondence between theory and observation in these cases was excellent.

5.4. *Effect of electrolyte type*

The effect of the valence type of the electrolyte upon the behaviour of the system may be examined by comparing runs 6 MC 3, 6 MC 6 and 6 MC 7. The data are summarized in tables 5 and 7. In this set of experiments the same pair of equivalent concentrations of a series of electrolytes was employed together with the same membrane.

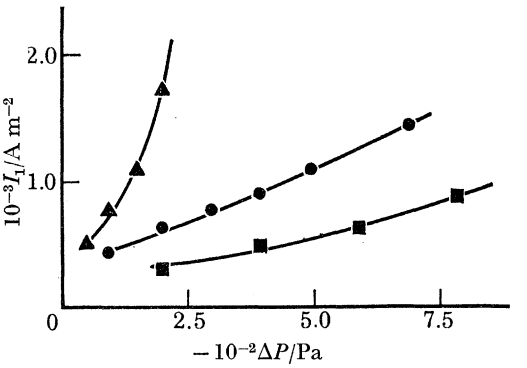

FIGURE 17. Observed flip currents I_1 plotted against applied pressure differential ΔP for run 6MC6 (▲), run 6MC3 (●), and run 6MC7 (■).

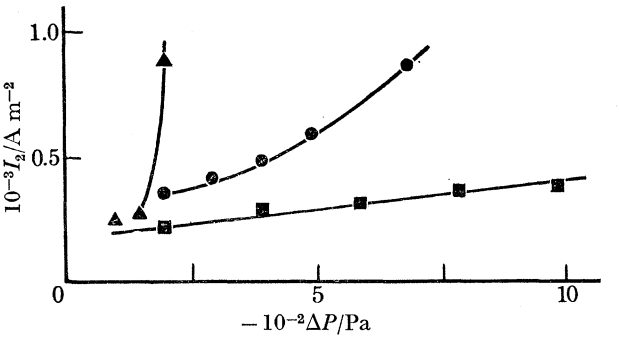

FIGURE 18. Observed flop currents I_2 plotted against applied pressure differential ΔP for run 6MC6 (▲), run 6MC3 (●), and run 6MC7 (■).

There was evidence that the surface charge on the pore walls arose from the adsorption of anions on to the non-ionogenic polymer surface. The important influences of changing the valence type of the electrolyte were therefore likely to be the dependence of K upon the adsorption, and hence the type of anion, and the dependence of the electro-osmotic permeability upon both K and the ionic strength of the solutions.

The same anions Cl^- were present in runs 6 MC 3 and 6 MC 6. Table 5 shows that K was effectively the same for NaCl and $MgCl_2$. The only effect on the membrane properties should be a consequence of the higher ionic strength of the $MgCl_2$ solutions leading to a lower electro-osmotic permeability. Figures 17 and 18 show that the effect of ionic strength on electro-osmotic permeability in these runs 6 MC 6 and 6 MC 3 was as predicted by the theory. I_1, I_2 and their slopes versus ΔP were larger in the case of $MgCl_2$.

The use of sulphate ions should lead to an increase in K and table 5 shows this was observed. This caused an enhancement of the electro-osmotic permeability in run 6 MC 7 which was countered somewhat by the higher ionic strength of the Na_2SO_4 solutions at the same equivalent concentration as the NaCl. In figures 17 and 18 it is seen that the enhancement of K decreased I_1 and I_2, and also the sensitivity to ΔP, when compared with run 6 MC 6, in which the ionic strengths were the same, and in 6 MC 3 in which they were lower.

The discrepancies between the observed and predicted values of I_1 were worse than in the case of I_2. In runs 6 MC 6 ($MgCl_2$) and 6 MC 7 (Na_2SO_4) this might have arisen because the theory neglected non-ideality of the solution in the pores. The errors from this assumption would be greatest when the pores were filled with the more concentrated solutions containing bivalent ions.

5.5. *Effect of electrolyte concentrations*

Runs 6 MC 2, 6 MC 3, 6 MC 4 and 6 MC 5, summarized in tables 5 and 7, demonstrate the effect of varying the concentrations of the electrolyte solutions in experiments on a single

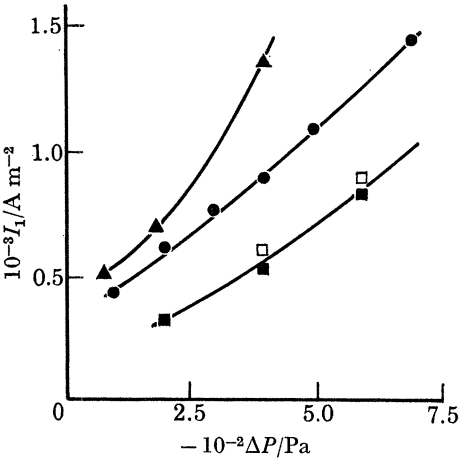

FIGURE 19. Observed flip currents I_1 plotted against applied pressure differential ΔP for run 6MC2 (▲), run 6MC3 (●), run 6MC4 (■), and run 6MC5 (□).

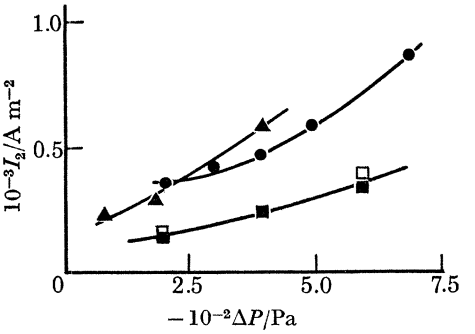

FIGURE 20. Observed flop currents I_2 plotted against applied pressure differential ΔP for run 6MC2 (▲), run 6MC3 (●), run 6MC4 (■), and run 6MC5 (□).

membrane. In these runs L_p and K were constant but the electro-osmotic permeability was varied by the alterations in the electrolyte concentrations.

Increasing the concentration had a twofold effect upon the electro-osmotic permeability. It increased the surface charge proportionally to $c^{\frac{1}{2}}$, and it decreased the thickness of the electrical double-layer which is inversely proportional to the square root of the ionic strength. As shown in equation (2.3.13) the combination of these effects leads to the electro-osmotic permeability being inversely proportional to the sixth root of the concentration of the solution in the pore. An increase in the concentration inside the membrane pores should therefore slightly decrease the electro-osmotic permeability and thereby increase I_1, I_2 and the sensitivity of the system to pressure changes.

Before the transition marked by I_1 the membrane pores are mainly filled with the concentrated solution while the reverse is true for the transition marked by I_2. In runs 6 MC 2 and 6 MC 3 the concentrated solution was 0.1 mol dm^{-3} NaCl in both cases and it would be expected that the values of I_1 would be about the same in both. The values of I_1 in runs 6 MC 4 and 6 MC 5 should be smaller and show less pressure sensitivity because in these the pores were filled with approximately 0.05 mol dm^{-3} NaCl immediately before the transition.

The same line of reasoning may be applied to the values of I_2. They should be similar for runs 6 MC 2, 6 MC 4 and 6 MC 5, where the pores were filled with approximately 0.005 mol dm^{-3} NaCl, and higher, with greater pressure sensitivity, for run 6 MC 3 where the pores contained 0.01 mol dm^{-3} NaCl before the transition. Figures 19 and 20 show that in general these predictions were borne out by experiment with the exception of I_2 in run 6 MC 2. This experiment differed from the others in that there was a twentyfold concentration ratio across the membrane instead of the tenfold ratio used in the other three runs.

5.6. *Mechanism of the flip-flop transition*

A possible explanation of the discrepancy noted in § 5.5 may be found by considering in detail the mechanism of the flip and flop transitions. Borsellino (1964) pointed out that during a transition the system passes through a state in which the volume flow in the centre of the pore, driven by the pressure differential, is oppositely directed from that adjacent to the pore wall, driven by electro-osmosis. Thus around the transition region concentrated solution is entering the centres of the pores at the high pressure end and dilute solution is entering the peripheries at the low pressure end. Ordinarily the radial concentration gradients thus created will be smeared out by radial diffusion after only a short interval along the pore from the open ends. When, however, the pores are not extremely long compared with their diameters (in the present case the ratio was about 12 : 1) and the pressure difference is high, giving rapid axial flow, the concentrated axial column may not be entirely dispersed by radial diffusion during the time of transit through the pore. The resulting 'break through' of concentrated solution to the dilute side would provide an electric current path of low resistance and the current density would be higher on the axis than at the periphery of the pore.

In the theory given here the local concentration is averaged over the pore cross-section and thus a uniform distribution of the current in the pores is implicitly assumed. If the current is distributed so that its density is higher in the centre of the pore, the average current density is greater than the density at the periphery. The prediction of a transition I_1 or I_2 means, in effect, the prediction of the current density at the pore periphery, where the electro-osmosis is generated, sufficient to produce a flow almost balancing the pressure driven flow. With this

current distribution the average current density required to produce the correct density at the periphery is greater than that predicted by the uniform current–density theory.

In the case of the I_1 transition the pore is already filled with concentrated solution and the transition involves insinuating a cylinder of dilute solution along the walls against the oncoming flow and the effects of radial diffusion. Except over a narrow front the current distribution may in this case be fairly uniform. In the case of the I_2 transition the pore is filled with a dilute solution and the transition involves insinuating a column of concentrated solution along its centre. It is in this case the breakthrough is most likely to occur. When the concentration ratio between the pore ends is large the non-uniform distribution of current caused by a tendency to break through will be most serious which may explain why this discrepancy was most apparent for I_2 in run 6 MC 2, the only one in which a 20 : 1 concentration ratio was used. In general, however, it has been found that the observed values of I_1 and I_2 tend to exceed those predicted.

The procedure adopted in the development of the theory of averaging the concentration over the pore cross-section at all distances before integrating across the membrane precludes the possibility of obtaining information on the detailed kinetics of flip and flop transitions. The discussion by Borsellino (1964) contained an attempt to rectify this deficiency.†

5.7. *The importance of the stagnant films*

A particular feature of the treatment used here is the allowance made for stagnant films of solution at the membrane faces. As an example, the importance of the concentration polarization

TABLE 8. EFFECT OF POLARIZATION OF STAGNANT LAYERS ON PREDICTIONS FOR RUN 6 MC 3

type of transition	predicted with no polarization / A m^{-2}	predicted with polarization / A m^{-2}	observed / A m^{-2}	ρ_{I}^m‡ / kg m^{-3}	ρ_{II}^m‡ / kg m^{-3}	$\rho_{\mathrm{I}}^m/\rho_{\mathrm{II}}^m$	$-\Delta P$ / Pa
I_1	none	309	439	1.16	4.54	0.255	98.1
I_2	none	282	none	0.782	3.10	0.252	98.1
I_1	473	554	627	1.76	5.29	0.333	196
I_2	469	361	356	0.745	2.47	0.301	196
I_1	651	886	771	2.17	5.57	0.391	294
I_2	565	434	414	0.739	2.22	0.333	294

‡ Unpolarized bulk concentrations, i.e. ρ_{I} and ρ_{II}, in all cases 0.733 and 5.98 kg m^{-3}; concentration ratio $\rho_{\mathrm{I}}/\rho_{\mathrm{II}} = 0.123$.

across these films is illustrated in table 8 for run 6 MC 3. It will be seen that polarization caused the dilute concentration ρ_{I}^m to be greater than ρ_{I} in the bulk solution and ρ_{II}^m to be smaller than ρ_{II}. For positive values of the volume flux the polarization had greater effect on the value of ρ_{II}^m. This enhanced the influence of the electrical double layers and so caused an increase in the electro-osmotic permeability and a consequent lowering of I_2. The opposite effect occurred for negative values of volume flow, thus leading to a raising of I_1. The stagnant films therefore increased the difference between I_1 and I_2.

In the case of run 2 MA the theory failed to predict flip-flop phenomena for the five lowest values of ΔP unless an allowance was made for the presence of stagnant films.

The electrical resistances of the two stagnant films contributed to the total resistance R

† The authors are grateful to Professor Borsellino for showing them the details of his treatment.

PHILOSOPHICAL TRANSACTIONS OF THE ROYAL SOCIETY A MATHEMATICAL, PHYSICAL & ENGINEERING SCIENCES

measured between the probe electrodes. As illustrated by the data in table 9*a* taken from run 6 MC 3 at $\Delta P = -98.1$ Pa, their contribution was small in terms of the absolute resistance. The membrane resistance R_m and the stagnant film resistances $R_{\delta I}$ and $R_{\delta II}$ were calculated separately and are included in table 9*a*. The calculations were made in the regions of large positive and large negative volume flows where the resistances are practically independent of the volume flow. The total resistance R_1 of the stirred layers between each probe and the stagnant film adjacent to it was then estimated by subtracting R_m, $R_{\delta I}$ and $R_{\delta II}$ from the observed value of R. It was not possible to measure R_1 directly owing to the uncertainty in the positions of the probes with respect to the membrane but the table shows that R_1 comprised from 60 to 90 % of the total resistance.

TABLE 9. CONTRIBUTIONS TO TOTAL RESISTANCE FOR RUN 6 MC 3

(*a*) *Breakdown of total resistance for* $\Delta P = -98.1$ Pa

	$10^5 V_m$/m s^{-1} − 5.60		$10^5 V_m$/m s^{-1} + 5.60	
type of resistance	resistance / 10^{-4} Ωm^2	% of total resistance	resistance / 10^{-4} Ωm^2	% of total resistance
R_1	67.0	91.5	68.1	61.4
$R_{\delta I}$	1.4	1.9	7.6	6.9
$R_{\delta II}$	0.9	1.2	3.8	3.4
R_m	3.9	5.3	31.5	28.4
R	73.2	—	111	—

(*b*) *Breakdown of resistance changes for several values of* ΔP

$-\Delta P$ / Pa	ΔR_m / 10^{-4} Ωm^2	ΔR_δ / 10^{-4} Ωm^2	total ΔR (calc.) / 10^{-4} Ωm^2	total ΔR (obs.) / 10^{-4} Ωm^2	total ΔR (calc. for no polarization) / 10^{-4} Ωm^2
98.1	27.6	9.0	36.6	37.8	23.1
392	27.7	9.0	36.7	44.2	23.1
687	27.7	9.0	36.7	36.8	23.1

Although the stagnant films made only a small contribution to the total resistance, their contribution to the resistance change ΔR was important. This is shown in table 9*b* where the calculated changes in membrane resistance ΔR_m and in the stagnant film resistance ΔR_δ are compared with the calculated and observed ΔR for run 6 MC 3. It is seen that ΔR_δ contributed about 25 % of ΔR. If it had not been included the correlation between the calculated and observed ΔR would have been much poorer.

5.8. *Nonlinearity of volume and ion fluxes*

The satisfactory agreement which has been demonstrated above between the observed and predicted electrical properties of this membrane system encourages confidence in the general correctness of the theoretical treatment. Although it has not yet been possible to measure either the volume flux or the individual ion fluxes they can be predicted from the theoretical equations. It is interesting and instructive to examine how these fluxes are expected to behave.

The values of the volume flux density V_m are plotted in figures 21 and 22 against the current per unit area of membrane I_m under the conditions of run 2 MA at two values of ΔP. The transition currents I_1 and I_2 are also marked on these diagrams.

An important feature concerning the stability of the system is the location of the condition of

zero volume flow $V_m = 0$. It may be identified with the aid of equation (2.3.15) which gives

$$(\Delta P)_{\bar{v}=0} = \frac{48K}{a^2\beta\Lambda}\left[\left(\frac{1}{\rho_I^m}\right)^{\frac{1}{6}} - \left(\frac{1}{\rho_{II}^m}\right)^{\frac{1}{6}}\right]\left[\Lambda' + \frac{I_m l}{\pi a^2 N(\rho_{II}^m - \rho_I^m)}\right] \quad (\rho_I^m \neq \rho_{II}^m) \tag{5.8.1}$$

for the relation between ΔP and I_m when $V_m = 0$.

It can be seen from figure 21, when ΔP is low, that starting from zero current where V_m is negative, the condition of $V_m = 0$ is passed before the transition I_1 is reached. In contrast figure 22 shows that at higher ΔP, $V_m = 0$ is located on the part of the curve which is inaccessible under galvanostatic conditions, that is, on a point beyond I_1.

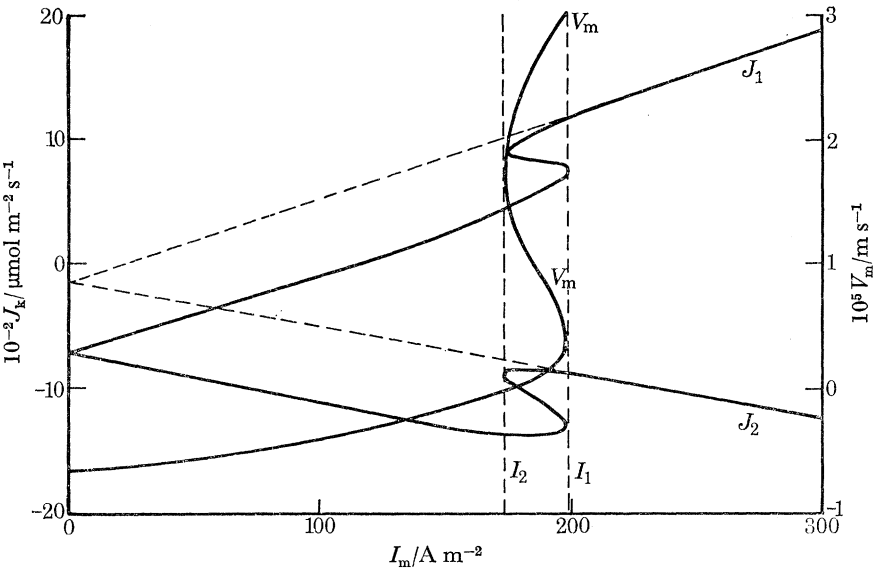

FIGURE 21. Predicted ion fluxes J_1 and J_2, and volume flow V_m plotted as functions of current I_m for run 2MA. The applied pressure differential was -294 Pa.

The effect of ΔP on the position of $I_m(V_m = 0)$ relative to I_1 may be understood by referring to the behaviour of the concentration profiles in the membrane pores. The concentration at a distance x through a pore may be obtained by integrating equation (2.3.21) from $x = 0$ to $x = x$. Under the restriction $\bar{v} \neq 0$, this gives

$$\rho_x = \left[\frac{(\rho_{II}^m - \rho_I^m)}{\exp(\bar{v}l/D_s) - 1}\right]\exp(\bar{v}x/D_s) - (\alpha/\bar{v}), \tag{5.8.2}$$

where α is given by equation (2.3.22).

Thus when $\bar{v}$ is not zero the profile in a pore has an exponential form. If $\bar{v} = 0$, equation (2.3.21) integrates to give

$$\rho_x = \rho_I^m + x(\rho_{II}^m - \rho_I^m)/l \tag{5.8.3}$$

and the profile is linear.

When ΔP is small the profile departs only slightly from linearity at $I_m = 0$ and this state persists as I_m is increased until V_m becomes slightly positive. The major changes in the profile take place over the region of currents where V_m increases from slightly to strongly positive; I_1 is therefore located in this region.

When ΔP is large, V_m is large and negative at $I_m = 0$, and the concentration profile in the pores is very far from linear. Most of each pore is filled with concentrated solution, and on increasing the current a large change in the profile towards linearity takes place as $V_m = 0$ is

approached. The flip-over at I_1 is triggered by this change and occurs before the condition $V_m = 0$ is reached, i.e. while the volume flux is still negative.

The molar fluxes of cations and anions J_1 and J_2 may be expressed in terms of the flows through unit area of membrane with the aid of equations (2.1.12), (2.1.14) and (2.1.15). These may be combined to give

$$J_1 = \pi a^2 N(\nu_1 \boldsymbol{J}_s/M_s + \boldsymbol{i}/\nu F), \tag{5.8.4}$$

and

$$J_2 = \pi a^2 N(\nu_2 \boldsymbol{J}_s/M_s - \boldsymbol{i}/\nu F); \tag{5.8.5}$$

J_1 and J_2 can therefore be calculated from the specific salt flux $\boldsymbol{J}_s$ and the electric current $\boldsymbol{i}$.

Figures 21 and 22 show the results of these calculations for two pressure differentials of run 2 MA. The graphs have very striking reversed Z-shapes. Before discussing these it is useful to re-express equations (5.8.4.) and (5.8.5) with the aid of equations (2.2.23), (2.2.24) and (2.3.8). This gives

$$J_1 = t_1 I_m - \nu_1 \pi a^2 N \boldsymbol{\alpha}/M_s \tag{5.8.6}$$

and

$$J_2 = -t_2 I_m - \nu_2 \pi a^2 N \boldsymbol{\alpha}/M_s. \tag{5.8.7}$$

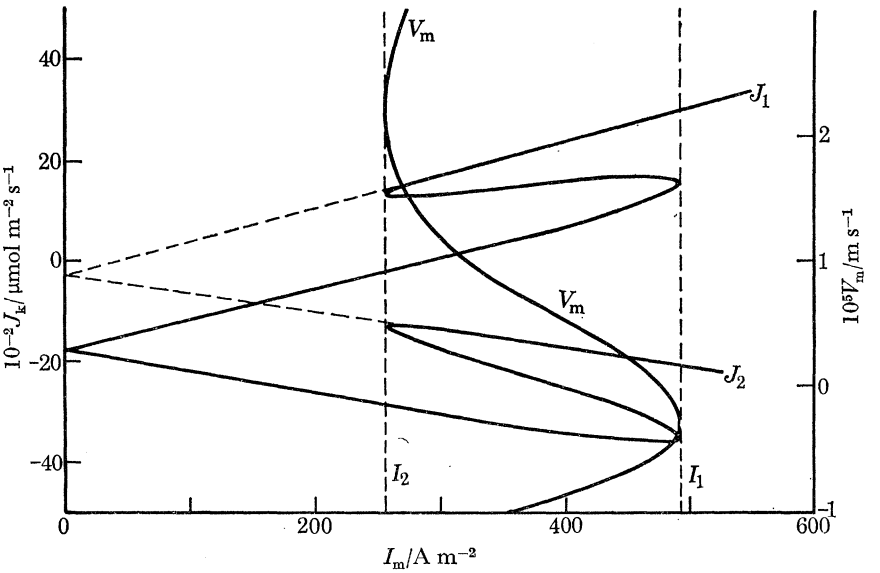

FIGURE 22. Predicted in fluxes J_1 and J_2, and volume flow V_m plotted as functions of current for run 2 MA. The applied pressure differential was −785 Pa.

Here t_1 and t_2 are cation and anion transport numbers and are related to the mobilities by

$$t_1 = \nu_2 u_1/(\nu_2 u_1 + \nu_1 u_2) \tag{5.8.8}$$

and analogously for t_2.

Consider first two extreme conditions; large and negative volume flow, and large and positive volume flow. Under the former the membrane pores can be considered to be filled with bulk solution ρ_{II} and under the latter with bulk solution ρ_I. Direct integration of equation (2.2.5), with subsequent elimination of $\Delta\psi$ under the restriction of constant concentration gives

$$\bar{\boldsymbol{v}} = \frac{a^2 \Delta P}{8\eta l} - \frac{K I_m}{\beta \eta \Lambda \pi a^2 N \rho^{\frac{2}{6}}}, \tag{5.8.9}$$

where for the first extreme condition $\rho = \rho_{II}$ and for the second $\rho = \rho_I$.

It can be seen from equation (2.3.22) that $\boldsymbol{\alpha}$ has limiting values of $-\bar{\boldsymbol{v}}\rho_{II}$ for $\bar{\boldsymbol{v}}$ negative, and $-\bar{\boldsymbol{v}}\rho_I$ for $\bar{\boldsymbol{v}}$ positive. Equations (5.8.6) and (5.8.7) can therefore be written for $\bar{\boldsymbol{v}}$ large and

negative and $\nu_1 = \nu_2 = 1$ in the form

$$J_1 = \frac{\pi a^4 N \rho_{\mathrm{II}}}{8\eta l M_{\mathrm{s}}} \Delta P + \left(\frac{t_1}{F} - \frac{K}{\beta \eta \Lambda M_{\mathrm{s}} \rho_{\mathrm{II}}^{\frac{1}{6}}} \right) I_{\mathrm{m}}, \tag{5.8.10}$$

$$J_2 = \frac{\pi a^4 N \rho_{\mathrm{II}}}{8\eta l M_{\mathrm{s}}} \Delta P - \left(\frac{t_2}{F} + \frac{K}{\beta \eta \Lambda M_{\mathrm{s}} \rho_{\mathrm{II}}^{\frac{1}{6}}} \right) I_{\mathrm{m}}, \tag{5.8.11}$$

and for $\bar{v}$ large and positive in the form

$$J_1 = \frac{\pi a^4 N \rho_{\mathrm{I}}}{8\eta l M_{\mathrm{s}}} \Delta P + \left(\frac{t_1}{F} - \frac{K}{\beta \eta \Lambda M_{\mathrm{s}} \rho_{\mathrm{I}}^{\frac{1}{6}}} \right) I_{\mathrm{m}}, \tag{5.8.12}$$

$$J_2 = \frac{\pi a^4 N \rho_{\mathrm{I}}}{8\eta l M_{\mathrm{s}}} \Delta P - \left(\frac{t_2}{F} + \frac{K}{\beta \eta \Lambda M_{\mathrm{s}} \rho_{\mathrm{I}}^{\frac{1}{6}}} \right) I_{\mathrm{m}}. \tag{5.8.13}$$

Plots of the ion fluxes versus current therefore tend towards straight lines at extreme values of the volume flow.

The criterion of each limiting condition is provided by equation (2.3.22). The first will be approached when

$$-\bar{v} l / D_{\mathrm{s}} \gg 1, \tag{5.8.14}$$

and the second when

$$\bar{v} l / D_{\mathrm{s}} \gg \ln (\rho_{\mathrm{II}}^m / \rho_{\mathrm{I}}^m). \tag{5.8.15}$$

In the examples plotted in figures 21 and 22 the largest positive volume flow employed in calculating the fluxes was 16 D_{s}/l whereas $\ln \rho_{\mathrm{II}}^m / \rho_{\mathrm{I}}^m$ was only 0.02 and the limiting condition was virtually reached. In fact the plots of J_1 and J_2 against I_{m} are seen to be linear for $I_{\mathrm{m}} > I_1$ because $\bar{v}$ jumps to quite large positive values at flip-over. The slopes are 6.66 and $-3.73\,\mu\mathrm{mol\,C^{-1}}$ at $\Delta P = -294\,\mathrm{Pa}$, and 6.75 and -3.65 at $\Delta P = -785\,\mathrm{Pa}$. At both pressures these correspond closely to the calculated limiting slopes 6.61 and $-3.74\,\mu\mathrm{mol\,C^{-1}}$.

The limiting condition for $\bar{v}$ large and negative was less well fulfilled. At $I_{\mathrm{m}} = 0$ and $\Delta P = -294\,\mathrm{Pa}$, $-\bar{v} l / D_{\mathrm{s}}$ was only 1.27 and at $\Delta P = -785\,\mathrm{Pa}$ it was 3.49. Despite this the plots of J_1 and J_2 versus I_{m} are surprisingly linear. If ρ_{II}^m were constant the plots would curve upwards over this range. This tendency is offset here by the decrease of ρ_{II}^m in the stagnant layer as $\bar{v}$ becomes less negative. The slopes of J_1 and J_2 versus I_{m} were 6.30 and $-3.96\,\mu\mathrm{mol\,C^{-1}}$ at $\Delta P = -294\,\mathrm{Pa}$ and 6.20 and -4.20 at $\Delta P = -785\,\mathrm{Pa}$. The theoretical limits are 5.90 and $-4.46\,\mu\mathrm{mol\,C^{-1}}$.

The discrepancies are not inappreciable when it is borne in mind that $\mathrm{d}J_1/\mathrm{d}I_{\mathrm{m}}$ always contains a contribution of $4.07\,\mu\mathrm{mol\,C^{-1}}$ from t_1/F and $\mathrm{d}J_2/\mathrm{d}I_{\mathrm{m}}$ contains -6.28 from $-t_2/F$. The discrepancies are due to true limits not being reached at $I_{\mathrm{m}} = 0$. They have the effect of making the linear portions of the graphs at I_{m} below the transition region not far from parallel to those above it.

Equations (5.8.6) and (5.8.7) show that $\mathrm{d}(J_1 - J_2)/\mathrm{d}I_{\mathrm{m}}$ must always be $1/F$ for uni-univalent electrolyte. Because the limiting conditions are not exactly attained the intercepts predicted by equations (5.8.10) to (5.8.13) at $I_{\mathrm{m}} = 0$ are slightly less negative than those observed in figures 21 and 22.

Over the range of I_{m} between I_1 and I_2, V_{m} has in principle three possible values although only two are accessible galvanostatically. Consequently α and hence J_1 and J_2 are all multi-valued over this range of current densities. This accounts for the reversed Z-shape of the J_1 and J_2 curves.

This analysis has emphasized that the ion fluxes follow a rather simple, if unusual, pattern as the current is increased from well below to well above the flip-flop region and that the features

peculiar to this membrane system are adequately accounted for by the sensitivity of the volume flux to the conflicting requirements of Poiseuille flow and electro-osmosis.

The authors wish to thank Mr I. Moir of the Department of Botany, University of Aberdeen, for his valuable assistance in the use of the projection microscope. They are very grateful to Dr J. D. Pryce of the Aberdeen University Mathematics Department for the explicit integration of equation (2.3.14).

References

Benton, D. P. & Elton, G. A. H. 1958 *Proc. 2nd Int. Congr. of Surface Activity* **3**, 28.
Borsellino, A. 1964 unpublished; reported at Gordon Conference, N.H., U.S.A.
Brown, A. S. 1934 *J. Am. chem. Soc.* **56**, 646.
De Groot, S. R. & Mazur, P. 1962 *Non-equilibrium thermodynamics*. Amsterdam: North Holland Publishing Co.
Drouin, H. 1969 *Ber. Bunsenges Phys. Chem.* **73**, 223.
Franck, U. F. 1963 *Ber. Bunsenges Phys. Chem.* **67**, 657.
Franck, U. F. 1967 *Ber. Bunsenges Phys. Chem.* **71**, 789.
Greenwood, J. A. 1968 *Proc. Instn elect. Engrs* **115**, 1717.
Gunning, H. E. & Gordon, A. R. 1942 *J. chem. Phys.* **10**, 126.
Harned, H. S. & Owen, B. B. 1960 *The physical chemistry of electrolyte solutions* (2nd. edn.). New York: Reinhold Publishing Corp.
Jancke, H. 1962 Dissertation. Technische Hochscule Darmstadt.
Katachalsky, A. & Curran, P. F. 1965 *Non-equilibrium thermodynamics in biophysics*. Harvard University Press.
Kobatake, Y. & Fujita, H. 1964 *J. chem. Phys.* **40**, 2212.
Kuhn, W., Läuger, P., Voellmy, H., Bloch, R. & Majer, H. 1963 *Ber. Bunsenges. Phys. Chem.* **67**, 364.
McHardy, W. J., Meares, P., Sutton, A. H. & Thain, J. F. 1969 *J. Colloid Interface Sci.* **29**, 116.
Mackay, D. & Meares, P. 1959 *Trans. Faraday Soc.* **55**, 1221.
McKeeman, W. M. & Tesler, L. 1963 *Collected algorithms from CACM*, algorithm no. 182.
Mikulecky, D. C. & Caplan, S. R. 1966 *J. phys. Chem.* **70**, 3049.
Oliva, G. A. 1967 *Gruppo Nazionale di Cibernetica C.N.R.*, no. 17.
Scattergood, E. M. & Lightfoot, E. N. 1968 *Trans. Faraday Soc.* **64**, 1135.
Schlögl, R. 1964 *Stofftransport durch Membranen*. Darmstadt: Steinkopff Verlag.
Teorell, T. 1951 *Z. Electrochem.* **55**, 460.
Teorell, T. 1959*a* *J. gen. Physiol.* **42**, 831.
Teorell, T. 1959*b* *J. gen. Physiol.* **42**, 847.

PHILOSOPHICAL TRANSACTIONS OF THE ROYAL SOCIETY A MATHEMATICAL, PHYSICAL & ENGINEERING SCIENCES